Geochemistry Geophysics Geosystems G3
AN ELECTRONIC JOURNAL OF THE EARTH SCIENCES
Published by AGU and the Geochemical Society

Article
Volume 2
June 27, 2001
Paper number 2000GC000137
ISSN: 1525-2027

Tracing a mantle plume: Isotopic and trace element variations of Galápagos seamounts

Karen S. Harpp
Department of Geology, Colgate University, Hamilton, New York 13346 (kharpp@mail.colgate.edu)

William M. White
Department of Geological Sciences, Cornell University, Ithaca, New York 14853 (white@geology.cornell.edu)

[1] **Abstract:** Isotopic and trace element analyses of basalts dredged from across the Galápagos Platform confirm the previously established east facing horseshoe pattern of depleted geochemical signatures at the center of the archipelago and more enriched signatures along the periphery. Statistical analysis of the isotopic data indicates that geochemical variations in the Galápagos cannot be explained by mixing between only the plume and the depleted asthenosphere. Instead, four isotopically distinct end-members must be interacting to account for the subtleties of the Sr, Nd, Pb, and He isotopic data. Three of the components are geographically restricted: one in the south, one in the central region, and one in the north. These three plume components then mix with the fourth component, depleted mantle, which is indistinguishable from the MORB source. The central component resembles the high $^{3}He/^{4}He$ mantle reservoir that may be common to many plumes and has variously been called PHEM, FOZO, and **C** by others. Whereas this mantle reservoir appears to make a minor contribution to the composition of most hot spot systems, it may constitute the main body of the Galápagos plume. Geographic distribution of the end-members suggests that the plume is centered near Fernandina ~92°N but may be significantly diluted by depleted mantle even near the main conduit. The geochemically distinct end-members trace an eastward mantle flow, manifested as decreasing contributions of the plume in the direction of plate motion. The plume may be tilted by shear in the asthenosphere from plate motion and ambient mantle flow. As it is bent, the plume thermally entrains surrounding upper mantle, resulting in the horseshoe-shaped distribution of depleted and enriched material. The end-members may also outline a deep, strong lateral flow of mantle toward the Galápagos Spreading Center, supplying plume material to the ridge system. Overall, our results suggest that the Galápagos hot spot is both compositionally and dynamically complex owing to its tectonic setting adjacent to a mid-ocean ridge.

Keywords: Galápagos; hotspot; plume-ridge interaction; isotopes; rare Earth elements; mantle reservoir.

Index terms: Isotopic composition/chemistry; dynamics, convection currents and mantle plumes; composition of the mantle; trace elements.

Received December 15, 2000; **Revised** March 21, 2001; **Accepted** March 22, 2001; **Published** June 27, 2001.

Harpp, K. S., and W. M. White, 2001. Tracing a mantle plume: Isotopic and trace element variations of Galápagos seamounts, *Geochem. Geophys. Geosyst.*, vol. 2, Paper number 2000GC000137 [17,499 words, 17 figures, 7 tables, 3 appendix tables, 1 animation]. Published June 27, 2001.

Theme: Plume-Ridge Interaction **Guest Editor:** David Graham

1. Introduction

[2] Hot spots and the magmas they produce serve as effective probes into the Earth's deep interior. In contrast, mid-ocean ridges are the direct result of plate tectonic processes; consequently, their more geochemically depleted magmas permit examination of the shallower mantle. When magmas are produced in an environment influenced by both hot spots and mid-ocean ridges, the geochemically distinct magmas can act as tracers of mantle flow patterns, extent of mixing between the two sources, as well as lithospheric structure and dynamics. The Galápagos Islands provide a rare opportunity to study the dynamics of both the deep and shallow mantle, primarily because of their location adjacent to the Galápagos Spreading Center (GSC), a prominent E-W trending mid-ocean ridge system north of the archipelago (Figure 1).

[3] The Galápagos Islands emerge from an extensive, shallow submarine volcanic platform notable for abundant seamounts. The small aerial extent of the Galápagos Islands suggests that this plume is a relatively weak one and, as a result, may be subject to velocity shear in the upper mantle by eastward flowing asthenosphere and lithosphere. This shearing may cause surrounding asthenosphere to be entrained into the center of the plume [e.g., *Richards and Griffiths*, 1989]. Such a configuration has been invoked to explain the intriguing distribution of isotopic and trace element ratios in subaerial Galápagos lavas; volcanoes on the outer ring of the archipelago display typical ocean island geochemistry, while the central lavas are distinctly more MORB-like [*White and Hofmann*, 1978; *Geist et al.*, 1988; *White et al.*, 1993].

[4] In addition to the effects of the asthenosphere on the hot spot, geochemical evidence indicates that the Galápagos hot spot influences the composition of magmas produced along the Galápagos Spreading Center, although the precise mechanism is not well understood. Mid-ocean ridge basalts erupted along the GSC become progressively enriched toward the Galápagos Islands, reaching a broad, ~100 km wide maximum centered on 92°W and tailing off to more depleted signatures both east and west of this region [e.g., *Schilling et al.*, 1982; J.-G. Schilling and R. H. Kingsley, personal communication, 2000]. Several other enigmatic features contribute to the complexity of the Galápagos hot spot system, including a series of seamounts and islands trending NW-SE from the spreading center toward the archipelago (the Wolf-Darwin Lineament (WDL)), a dramatically steep escarpment marking the southern and western edges of the platform, two subparallel aseismic ridges emanating from the region (Carnegie and Cocos Ridges), and a group of elongated seamounts in the NE (Figure 1). Together, these factors make the Galápagos Archipelago a unique and particularly valuable location to study plume and mantle dynamics, plume source characteristics, and plume-ridge interactions.

[5] The PLUM02 Expedition was a multidisciplinary effort to study the Galápagos Platform [*Christie et al.*, 1992]. One of the primary goals was to determine whether the east facing horseshoe pattern of geochemical variations [*Geist et al.*, 1988] persists throughout the volcanic platform underlying the islands by collecting lavas from regional seamounts. Dredging in key locations more than doubled previous spatial coverage, including samples from the northeast region of the submarine platform (at the open end of the horseshoe pattern), the Wolf-Darwin Lineament (NW of the islands), the southwestern escarpment near the plume center, and locations "downstream" of the hot spot on the Carnegie Ridge (Figure 1).

[6] We report the results of a geochemical study of the dredged PLUM02 seamount sam-

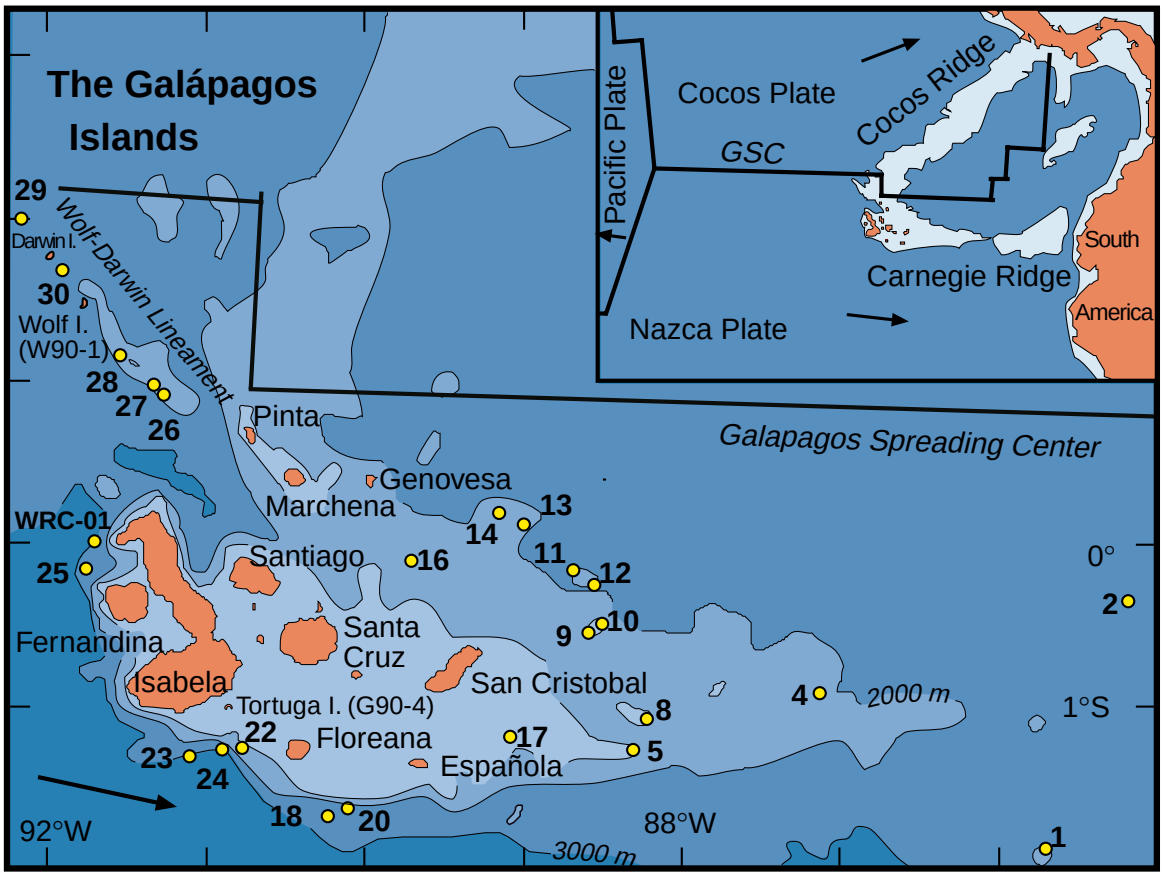

Figure 1. Map of Galápagos Platform. Inset shows regional tectonic setting. Solid yellow circles are PLUM02 dredge locations. GSC indicates the Galápagos Spreading Center, represented by the black solid and dashed lines north of the platform. The black arrow shows plate motion direction [*Gripp and Gordon*, 1990]. Contours are in 1000-m increments.

ples, including strontium, neodymium, and lead isotopic ratios as well as trace element concentrations. In our analysis we consider data of *White et al.* [1993], *Kurz and Geist* [1999], and *Graham et al.* [1993] along with our new submarine data for a comprehensive examination of plume source composition, plume-asthenosphere dynamics, and plume-ridge interactions in the Galápagos region. Our isotopic and trace element results from dredges across the Galápagos Platform confirm the previously established east facing horseshoe pattern of depleted geochemical signatures at the center of the archipelago and more enriched signatures along the northern, western, and southern periphery. Statistical analysis of the isotopic results suggests that four isotopically distinct mantle components contribute to Galápagos magmas: three of these components may be intrinsic to the plume, while the fourth is indistinguishable from the MORB source and is presumably the shallow asthenosphere.

2. Analytical Procedures

[7] Samples were collected in 1990 during dredging operations aboard the R/V *Thomas*

Table 1. Isotopic Standard Values[a]

	$^{87}Sr/^{86}Sr$	$^{143}Nd/^{144}Nd$	$^{143}Nd/^{144}Nd$	$^{206}Pb/^{204}Pb$	$^{207}Pb/^{204}Pb$	$^{208}Pb/^{204}Pb$
Standard	NBS 987	Ames	LaJolla	NBS 981	NBS 981	NBS 981
Mean	0.710223	0.512134	0.511852	16.902	15.446	36.558
s_a	0.000007	0.000007	0.000007	0.006	0.007	0.023
n	21	32	15	21	21	21

[a]Symbols are as follows: s_a, analytical standard deviation; n, number of analyses. Strontium isotope ratios were corrected for mass fractionation assuming a $^{86}Sr/^{88}Sr$ ratio of 0.1194 using an approximation of the exponential mass fractionation law. All results were corrected to an NBS 987 value of 0.710247. Neodymium isotope ratios were exponentially corrected for mass fractionation assuming a $^{146}Nd/^{144}Nd$ ratio of 0.721900. Both Ames and LaJolla standards yielded a $^{145}Nd/^{144}Nd$ of 0.348426. All results were corrected to a LaJolla standard value of 0.511847. Calculation of ε_{Nd} was based on a $^{145}Nd/^{144}Nd$ ratio of 0.512638 for chondritic uniform reservoir (CHUR). A fractionation correction was applied to all Pb isotopic analyses assuming true values for the NBS 981 standard of 16.937, 15.493, and 36.705.

Washington; a comprehensive map of the platform based on detailed SeaBeam mapping has been prepared [*Christie and Fox*, 1990]. Additional reports of the geochemical and geophysical PLUM02 results are given by *Christie et al.* [1992], *Sinton et al.* [1996], *Sinton et al.* [1993], *Graham et al.* [1993], *McBirney* [1993], and *Feighner and Richards* [1995a, 1995b].

[8] Of the 30 attempted dredges, 24 were successful, recovering mostly fresh, angular basalt pieces (Figure 1). Wherever collected, we sampled glassy rinds for subsequent analysis. In the laboratory, all samples were carefully handpicked to avoid alteration products. After sample selection, all further handling and chemistry procedures were carried out in a class 1000 clean room. All reagents used in analytical procedures were prepurified.

[9] Isotopic analyses were performed on two thermal ionization mass spectrometers (TIMS) in the Keck Isotope Lab of Cornell University: a VG Sector and its replacement, a Fisons VG Sector 54. Analyses of several identical sam-

Table 2. ICP-MS Values for USGS Geological Reference Materials[a]

	Ba	La	Ce	Pr	Nd	Sm	Eu	Gd	Tb	Dy	Ho	Er	Tm	Yb	Lu
BIR-1															
mean	6.6	0.65	1.89	0.39	2.39	1.10	0.49	1.91	0.38	2.52	0.58	1.63	0.26	1.63	0.26
s_a	0.3	0.06	0.08	0.02	0.09	0.05	0.02	0.10	0.02	0.10	0.03	0.07	0.02	0.07	0.02
n	45	46	46	46	46	46	46	46	46	46	46	46	46	46	46
DNC-1															
mean	105	3.74	8.19	1.13	5.04	1.45	0.60	2.16	0.42	2.79	0.65	1.87	0.30	1.97	0.32
s_a	3.1	0.12	0.33	0.04	0.17	0.06	0.02	0.10	0.02	0.10	0.03	0.07	0.01	0.09	0.01
n	56	58	58	58	58	58	58	58	58	58	58	58	58	58	58
W-2															
mean	172	10.7	23.4	3.07	13.2	3.31	1.10	3.91	0.68	3.92	0.81	2.18	0.33	2.08	0.33
s_a	5.0	0.30	0.8	0.11	0.40	0.12	0.04	0.11	0.02	0.10	0.03	0.06	0.01	0.08	0.02
n	69	75	75	75	75	75	75	75	75	75	75	75	75	75	75
BHVO-1															
mean	130	15.3	37.3	5.37	24.6	6.06	1.98	6.48	1.04	5.36	1.00	2.44	0.34	2.00	0.29
s_a	4.4	0.33	0.7	0.09	0.41	0.12	0.04	0.13	0.02	0.14	0.03	0.08	0.02	0.08	0.02
n	53	54	54	54	54	54	54	54	54	54	54	54	54	54	54

[a]Values are in ppm; s_a, analytical standard deviation; n, number of analyses.

ples were repeated on each instrument to verify analytical agreement between the mass spectrometers. Where standard means varied between instruments, samples were adjusted by the differential between the standard means. Standards are reported only for the new Sector 54 TIMS but are representative of both instruments (Table 1). Prior to separation procedures, all samples were leached with 2 M HCl for 10–60 min, depending on their level of visible alteration. Routine chemical separation procedures were followed and are described by *Harpp* [1995]. Procedural blanks were negligible for Sr and Nd and consistently less than 200 pg for Pb. Values listed in Table 2 represent means of two or more replicate analyzes.

[10] Concentrations of the rare earth elements and barium were determined by inductively coupled plasma-mass spectrometry (ICP-MS) using the VG Fisons Plasmaquad PQ2+ at Cornell University. Samples were dissolved to a thousand-fold dilution following the procedure outlined by *Harpp* [1995]. Data were collected using a nonlinear drift correction procedure and external calibration against matrix-matched standards as described by *Cheatham and Sangrey* [1993]. Standards are reported in Table 2.

3. Results

3.1. Isotope Ratios

[11] Lavas from single dredge sites are largely isotopically homogeneous, with the bulk of the variation occurring between, rather than within, dredges (Table 3); the only exceptions are PL02-13 and 26 lavas. In the subsequent discussion we utilize the means of results for each dredge location.

[12] Strontium, neodymium, and lead isotope ratios for the dredged lavas confirm and strengthen previous geochemical observations; the anomalous horseshoe-shaped pattern of depletion at the center and enrichment at the periphery of the archipelago is preserved (Figures 2, 3, and 4). Seamount lavas span the compositional range between ocean island basalts (OIB) and mid-ocean ridge basalts (MORB), similar to the island lavas. Perhaps the most surprising result is the markedly depleted isotopic signatures of northeast seamount lavas. Material from PL02-9 through PL02-14 has the most depleted isotopic signatures in the region and extends the Galápagos field well into MORB isotopic space, displaying some of the most depleted signatures detected in an ocean island setting to date. The NE lavas resemble those from Genovesa, a small northern island just south of the GSC [*Harpp et al.*, 2000].

[13] Wolf-Darwin Lineament samples (PL02-26 through 30) extend the field established by Wolf and Darwin Islands to MORB-like values. The depleted samples (from the SE end of the WDL) resemble northeast seamount lavas, whereas the more enriched material (NW end of lineament) clusters near data from the islands of Wolf, Darwin, and Pinta. In every case, however, ε_{Nd} values are lower for a given $^{87}Sr/^{86}Sr$ compared to southern archipelago lavas, where the low ε_{Nd} is defined by Pinta.

3.2. Trace Elements

[14] The PLUM02 lavas exhibit a wide variation in trace element compositions, ranging from light rare earth (LRE) enriched to LRE-depleted (Table 4, Figures 5 and 6), consistent with established patterns in the island data [*White et al.*, 1993]. Furthermore, trace element variations conform to previously established geographic patterns: (1) In the southwest, PL02-16 through 18, PL02-22 through 24, and Tortuga Island lavas reveal fairly uniform LRE-enriched patterns, with slightly gentler

Table 3. Isotopic Ratios for the PLUM02 Samples[a]

Samples	Location	$^{87}Sr/^{86}Sr$	$^{143}Nd/^{144}Nd$	ε_{Nd}	$^{206}Pb/^{204}Pb$	$^{207}Pb/^{204}Pb$	$^{208}Pb/^{204}Pb$
PL02-1-12	02°01.5′S 85°40.3′W	0.703081	0.513099	8.99	18.993	15.554	38.613
PL02-2-1	00°22.4′S 85°09.7′W	0.702995	0.513050	8.03	18.967	15.560	38.480
PL02-2-2	00°22.4′S 85°09.7′W	0.702929	0.513061	8.25	19.050	15.538	38.334
PL02-4-14	00°55.9′S 87°07.5′W	0.703305	0.513042	7.88	19.094	15.585	38.591
PL02-5-1	01°17.4′S 88°21.2′W	0.703152	0.513041	7.86	19.008	15.609	38.618
PL02-8-1	01°17.4′S 88°21.2′W	0.703038					
PL02-9-7	00°28.1′S 88°32.0′W	0.702723	0.513144	9.87	18.318	15.482	37.725
PL02-9-29	00°28.1′S 88°32.0′W	0.702646	0.513130	9.59	18.339	15.484	37.775
PL02-10-5	00°33.0′S 88°32.0′W	0.702795	0.513115	9.30	18.649	15.538	38.150
PL02-10-8	00°33.0′S 88°32.0′W	0.702702			18.758	15.584	38.554
PL02-11-5	00°11.7′S 88°40.1′W	0.702761	0.513111	9.23	18.766	15.541	38.290
PL02-12-1	00°12.8′S 88°39.2′W	0.702680	0.513114	9.28	18.603	15.557	38.221
PL02-12-1	00°12.8′S 88°39.2′W	0.702641	0.513126	9.51	18.790	15.629	38.692
PL02-13-4	00°04.6′N 89°02.7′W	0.702851	0.513118	9.36	18.505	15.522	37.959
PL02-13-25	00°04.6′N 89°02.7′W	0.702614	0.513116	9.32	18.760	15.603	38.624
PL02-14-8	00°04.1′N 89°07.1′W	0.702575	0.513153	10.05	18.396	15.490	37.854
PL02-16-3[b]	00°06.4′S 89°49.3′W	0.707220	0.512971	6.49	19.492	15.617	39.080
PL02-17-1	01°11.4′S 89°06.6′W	0.703146	0.513002	7.10	18.949	15.562	38.485
PL02-20-5	01°37.7′S 90°10.7′W	0.703434	0.512905	5.21	19.575	15.620	39.262
PL02-22-8	01°18.2′S 90°44.9′W	0.703436	0.512953	6.14	19.407	15.597	39.014
PL02-23-1	01°20.0′S 90°59.8′W	0.703463	0.512906	5.23	19.313	15.583	38.942
PL02-24-32	01°17.5′S 90°54.9′W	0.703370	0.512945	5.98	19.329	15.586	38.948
PL02-24-37	01°17.5′S 90°54.9′W	0.703428	0.512912	5.35	19.307	15.569	38.908
PL02-25-1	01°16.3′S 91°46.9′W	0.703319	0.512935	5.79	19.099	15.531	38.589
PL02-25-4	01°16.3′S 91°46.9′W	0.703298	0.512961	6.30	19.070	15.494	38.467
PL02-25-4	01°16.3′S 91°46.9′W				19.080	15.515	38.533
PL02-26-7	00°50.50′N 91°17.30′W	0.702793	0.512997	6.99	19.127	15.575	38.791

Table 3. (continued)

Samples	Location	$^{87}Sr/^{86}Sr$	$^{143}Nd/^{144}Nd$	ε_{Nd}	$^{206}Pb/^{204}Pb$	$^{207}Pb/^{204}Pb$	$^{208}Pb/^{204}Pb$
PL02-26-16	00°50.0′N 91°17.5′W	0.702838	0.513003	7.12	19.121	15.584	38.778
PL02-26-21	00°50.0′N 91°17.5′W	0.702831	0.513011	7.27	19.152	15.592	38.844
PL02-26-25[c]	00°50.0′N 91°17.5′W	0.702874	0.512994	6.94	19.161	15.582	38.766
PL02-26-25[d]	00°50.0′N 91°17.5′W	0.702605	0.513070	8.43			
PL02-27-1	00°52.8′N 91°19.6′W	0.702613	0.513086	8.73	18.641	15.516	38.076
PL02-27-17	00°52.8′N 91°19.6′W	0.702570	0.513044	7.93	18.617	15.482	37.975
PL02-28-1	01°01.5′N 91°33.3′W	0.702765	0.513038	7.79	19.067	15.588	38.673
PL02-28-11	01°01.5′N 91°33.3′W	0.702771	0.513037	7.78	19.028	15.564	38.602
PL02-29-2	01°54.0′N 92°09.7′W	0.702924	0.512995	6.97	18.963	15.546	38.713
PL02-29-3	01°54.0′N 92°09.7′W	0.702954	0.513008	7.22	19.001	15.599	38.895
PL02-30-1	01°35.5′N 91°55.6′W	0.703011	0.512964	6.37	19.366	15.620	39.282
PL02-W90-1	Wolf Island	0.703018	0.512983	6.72	19.135	15.604	39.028
PL02-WRC-1	00°13.9′S 91°45.3′W	0.703218	0.512940	5.88	19.075	15.533	38.632
PL02-G90-4	Tortuga Island	0.703420	0.512877	4.66	19.432	15.568	38.992

[a]All samples were carefully handpicked to avoid visible alteration products. Material was ultrasonically cleaned in distilled water prior to processing. Between 100 and 300 mg of glass chips were selected for isotopic analysis. After sample selection, all further handling and chemistry procedures were carried out in a class 1000 clean room. See *Harpp* [1995] for details.
[b]After rigorous leaching (>1 hour with 2 M HCl), sample PL02-16-3 yielded an elevated $^{87}Sr/^{86}Sr$ value of 0.70722, a distinctly altered signature. We have chosen to eliminate samples from dredge 16 from all further discussion.
[c]Crystalline portion of dredged sample.
[d]Glassy portion of dredged sample.

slopes than in the west. Lavas from PL02-20, despite being located near PL02-18, exhibit a distinctly concave-upward shape comparable to Floreana lavas (Figure 5) [*White et al.*, 1993]. The most steeply sloping REE patterns are found in the western lavas (e.g., PL02-25, Figure 5). (2) Lavas from the northeastern seamounts display a range of MORB-like REE patterns, extending to the most LRE-depleted material recovered from the archipelago thus far (PL02-9, 13, and 14; Figure 5). Most of these samples have LRE-depleted patterns with flat HRE slopes, similar to Genovesa lavas. (3) Wolf-Darwin Lineament samples vary from distinctly MORB-like to slightly LRE-enriched (Figure 6), with no obvious systematic pattern; that is, the most LRE-enriched lavas are found between Wolf and Darwin Islands at PL02-30, while the most depleted are observed at PL02-27, near the SE end of the lineament. (4) Samples dredged from along the Carnegie Ridge east of the islands display a wide range of REE patterns and absolute concentrations (Figure 6), from LRE-depleted (e.g., PL02-1–12, 19) to slightly LRE–enriched (PL02-2). Basalts from PL02-4 and PL02-5 are similar to lavas from nearby San Cristobal and Española.

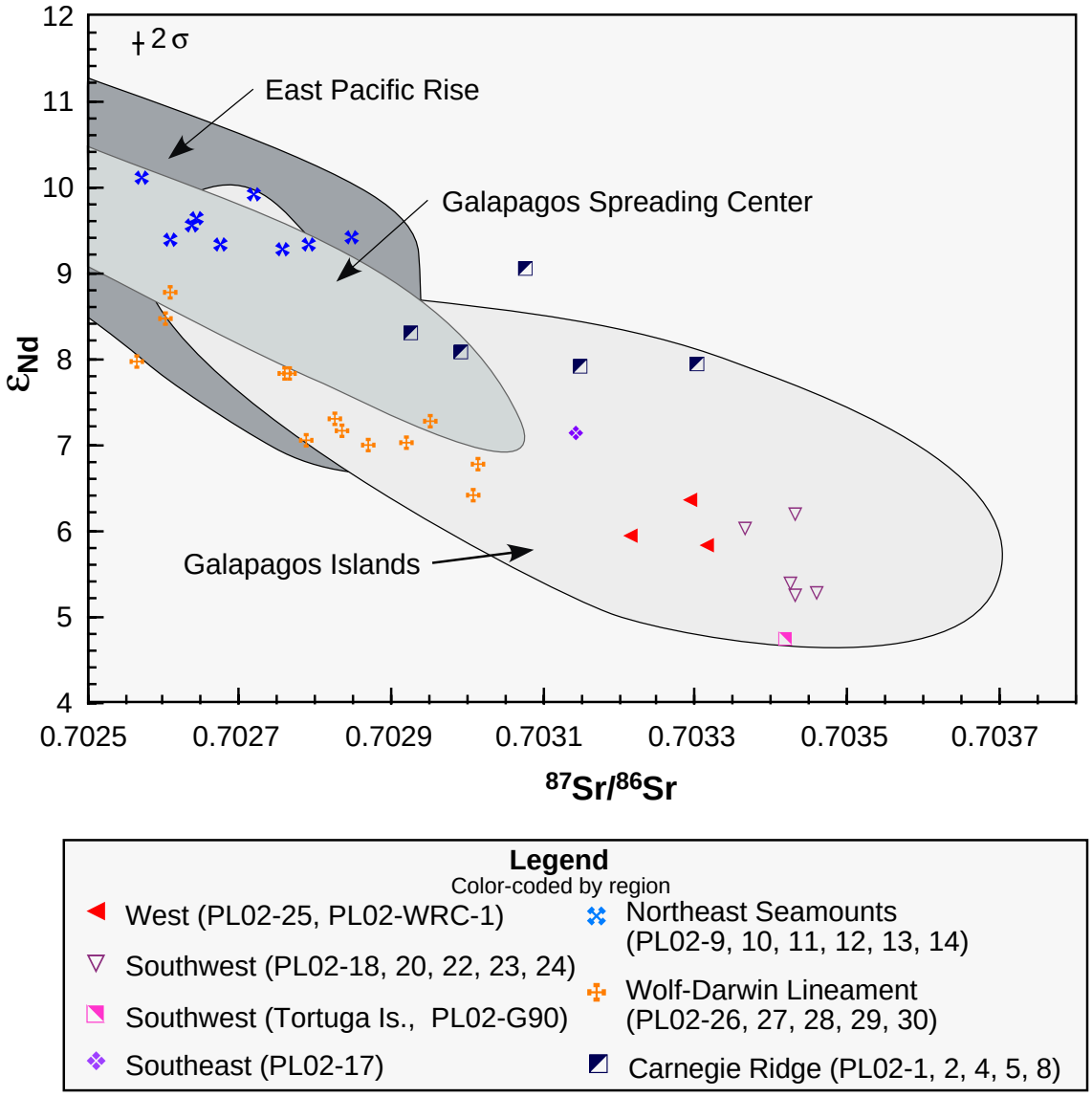

Figure 2. $^{87}Sr/^{86}Sr$ versus ε_{Nd} for PLUM02 data. See legend for symbols. Galápagos Island data by *White et al.* [1993]. Galápagos Spreading Center data by *Verma and Schilling* [1982], *Verma et al.* [1983], and J. G. Schilling and R. H. Kingsley, personal communication, 2000]. East Pacific Rise data by *Prinzhofer et al.* [1989], *Mahoney et al.* [1994], *Harpp* [1995] and E. Klein, personal communication, 1995. PL02-16 has not been included because of its high degree of alteration.

[15] Trace element concentrations and isotope ratios are well correlated (Table A1 available at http://www.g-cubed.org/publicationsfinal/article/2000GC000137/2000GC000137-a01.txt). Enriched isotopic signatures generally accompany LRE-enriched patterns. There are exceptions, however, particularly within certain regions. For instance, in the northeast seamounts, material from PL02-13 and PL02-14 have similar REE compositions, yet exhibit the

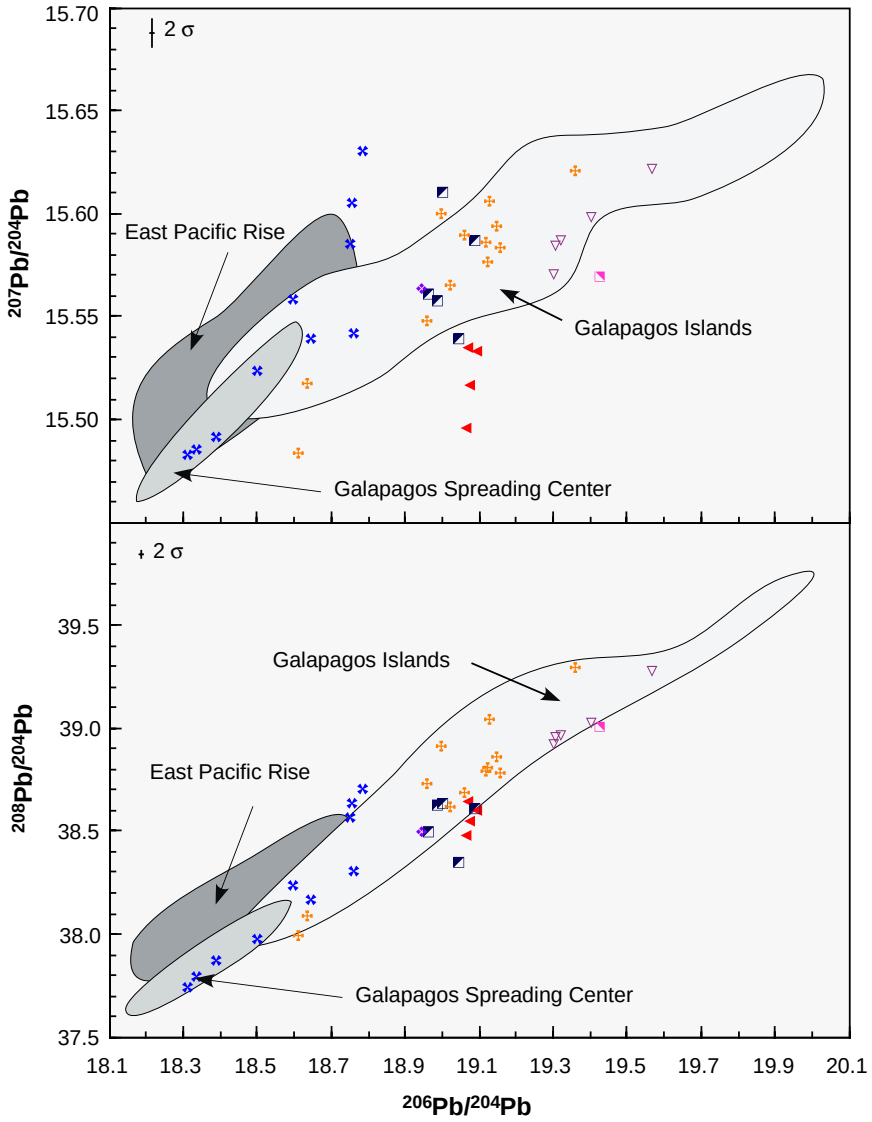

Figure 3. Pb isotopic variation diagrams for PLUM02 data. (a) $^{207}Pb/^{204}Pb$ versus $^{206}Pb/^{204}Pb$; (b) $^{208}Pb/^{204}Pb$ versus $^{206}Pb/^{204}Pb$. See Figure 2 for symbols and data sources.

most enriched and most depleted isotopic signatures in this area, respectively. Material from PL02-2 has somewhat depleted isotopic ratios and LRE-enriched REE patterns, whereas PL02-4 lavas are more isotopically enriched but LRE-depleted. Similar geochemical contradictions are observed throughout the island lavas [*White et al.*, 1993].

3.3. Geographic Patterns

[16] The distribution of isotopic ratios in the Galápagos is distinctive, as initially noted by *White and Hofmann* [1978]. Lavas with enriched isotopic and trace element signatures form an east facing horseshoe at the periphery of the archipelago, becoming more depleted at

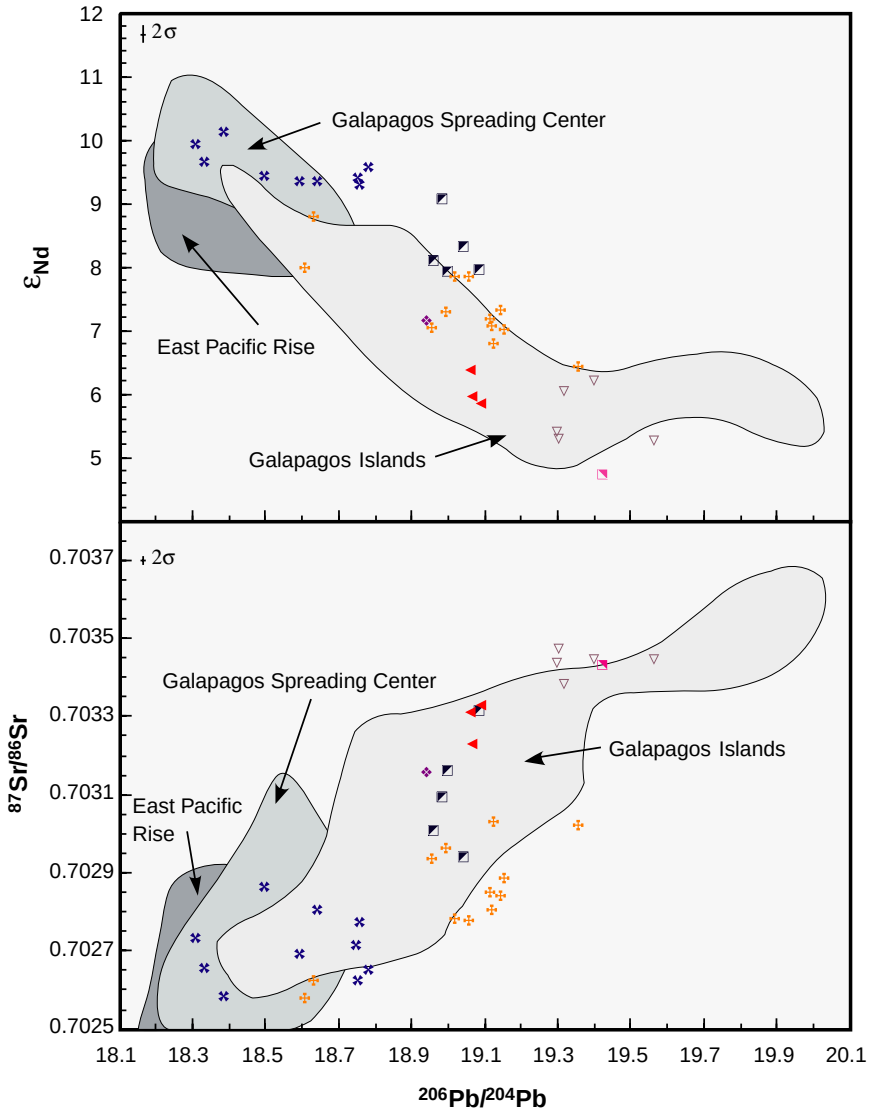

Figure 4. (a) $^{206}Pb/^{204}Pb$ versus ε_{Nd} for PLUM02 data; (b) $^{206}Pb/^{204}Pb$ versus $^{87}Sr/^{86}Sr$ for PLUM02 data. See Figure 2 for symbols and data sources.

the center [*White et al.*, 1993]. Our new results are remarkable in that they are not only entirely consistent with early observations based on sparse sub-aerial sampling (13 major islands and several islets), but the geochemical pattern appears to extend across the expansive submarine platform underlying the island chain (Figures 7–9).

4. Mantle Sources of Galápagos Lavas

4.1. Mantle Heterogeneity Beneath the Galápagos

[17] Although Sr, Nd, and Pb isotopic ratios have been affected by crustal assimilation at

Table 4. Trace Element Results for the PLUM02 Samples[a]

	Ba	La	Ce	Pr	Nd	Sm	Eu	Gd	Tb	Dy	Ho	Er	Tm	Yb	Lu	La/Sm_n	Sm/Yb_n
PL02-1-12	22.4	4.62	16.1	3.37	19.9	7.48	2.12	9.23	1.77	10.6	2.35	6.43	0.99	6.44	1.03	0.38	1.26
PL02-1-19	62.5	1.92	3.69	0.77	4.50	1.83	0.69	2.67	0.55	3.61	0.81	2.23	0.36	2.21	0.36	0.65	0.90
PL02-2-1	56.1	9.90	24.8	3.74	18.2	5.31	1.70	6.15	1.16	7.00	1.46	3.90	0.59	3.68	0.55	1.15	1.57
PL02-2-2	47.6	9.53	24.6	3.78	18.6	5.48	1.75	6.42	1.22	7.41	1.55	4.12	0.64	3.92	0.60	1.07	1.52
PL02-4-14	18.0	2.51	6.27	1.10	5.82	2.02	0.79	2.85	0.59	3.67	0.80	2.29	0.37	2.33	0.37	0.77	0.94
PL02-5-1	34.5	4.65	10.8	1.68	8.37	2.61	1.04	3.53	0.69	4.28	0.94	2.64	0.42	2.63	0.41	1.10	1.08
PL02-9-7	3.18	1.46	5.95	1.24	7.29	2.58	0.99	3.32	0.65	3.94	0.84	2.30	0.35	2.24	0.35	0.35	1.25
PL02-9-33	5.05	1.34	5.59	1.15	6.65	2.36	0.95	3.18	0.63	3.94	0.86	2.38	0.37	2.39	0.37	0.35	1.07
PL02-10-5	17.2	3.27	9.96	1.78	9.86	3.32	1.22	4.31	0.84	5.00	1.07	2.95	0.45	2.80	0.44	0.61	1.28
PL02-11-5	68.1	7.19	19.1	2.99	15.1	4.46	1.54	5.39	1.03	6.07	1.30	3.59	0.55	3.52	0.56	0.99	1.37
PL02-12-1	9.30	2.56	8.49	1.63	9.31	3.29	1.21	4.50	0.90	5.54	1.25	3.52	0.55	3.51	0.55	0.48	1.02
PL02-13-4	3.32	1.02	3.84	0.88	5.76	2.49	0.98	3.62	0.75	4.65	1.03	2.83	0.43	2.71	0.42	0.25	0.99
PL02-14-8	2.73	0.90	3.78	0.87	5.29	2.12	0.84	2.87	0.57	3.64	0.80	2.24	0.35	2.20	0.35	0.26	1.05
PL02-16-3	98.9	16.9	39.2	5.47	24.2	6.37	2.16	6.79	1.25	7.02	1.41	3.76	0.56	3.51	0.54	1.63	1.97
PL02-17-1	97.3	18.0	46.0	6.64	31.2	8.11	2.60	8.70	1.63	9.27	1.90	5.22	0.78	4.91	0.77	1.37	1.79
PL02-18-1	106	20.5	46.2	6.57	30.3	7.80	2.46	8.24	1.49	8.30	1.67	4.43	0.64	3.91	0.60	1.63	2.16
PL02-20-5	349	25.3	42.5	4.78	18.0	3.64	1.27	3.98	0.71	4.02	0.86	2.40	0.36	2.35	0.38	4.28	1.68
PL02-22-1	103	15.9	36.5	5.07	23.3	5.82	1.97	6.27	1.16	6.34	1.23	3.26	0.46	2.79	0.42	1.69	2.26
PL02-22-8	108	19.6	45.2	6.22	27.6	6.79	2.21	7.35	1.33	7.31	1.44	3.78	0.56	3.43	0.51	1.78	2.14
PL02-23-1	112	16.8	39.3	5.40	24.2	5.88	1.93	6.00	1.11	5.88	1.15	2.98	0.43	2.59	0.40	1.76	2.46
PL02-24-1	100	15.1	35.6	4.88	21.8	5.62	1.76	5.80	1.02	5.72	1.12	2.87	0.42	2.54	0.38	1.66	2.40
PL02-24-32	81.8	12.6	30.0	4.14	18.5	4.74	1.66	5.22	0.89	4.83	0.94	2.40	0.35	2.08	0.31	1.64	2.47
PL02-25-4	182	22.7	52.9	7.21	31.8	7.21	2.36	6.83	1.17	6.06	1.11	2.79	0.40	2.38	0.36	1.94	3.29
PL02-26-7	49.8	7.54	19.2	2.87	14.5	4.26	1.50	4.87	0.90	5.12	1.06	2.79	0.41	2.52	0.39	1.09	1.83
PL02-26-16	48.5	7.46	18.9	2.91	14.3	4.24	1.53	5.00	0.94	5.37	1.12	2.95	0.43	2.66	0.41	1.09	1.72
PL02-26-21	47.5	7.44	18.7	2.87	14.3	4.16	1.49	4.99	0.90	5.24	1.09	2.84	0.42	2.56	0.40	1.11	1.76
PL02-26-25	46.3	7.09	17.9	2.69	13.3	3.94	1.42	4.70	0.86	4.85	1.01	2.66	0.39	2.42	0.37	1.11	1.76
PL02-27-1	12.7	3.02	9.95	1.88	10.9	3.89	1.44	5.10	0.98	5.88	1.26	3.41	0.52	3.26	0.50	0.48	1.29
PL02-28-1	33.5	5.44	14.6	2.34	12.0	3.79	1.38	4.65	0.89	5.10	1.06	2.87	0.44	2.67	0.41	0.89	1.54
PL02-28-11	31.1	5.33	14.3	2.31	12.1	3.78	1.36	4.74	0.86	5.06	1.05	2.82	0.43	2.64	0.41	0.87	1.55
PL02-29-3	41.3	4.85	11.8	1.78	9.16	2.92	1.07	3.90	0.77	4.70	1.03	2.85	0.44	2.78	0.44	1.02	1.14
PL02-30-1	100	10.4	23.0	3.09	13.5	3.38	1.24	4.09	0.74	4.34	0.94	2.51	0.39	2.44	0.37	1.90	1.50
PL02-G90-4	118	18.4	42.9	5.98	26.3	6.44	2.16	6.58	1.19	6.62	1.29	3.34	0.48	2.94	0.43	1.76	2.38
PL02-G90-6	126	18.4	43.5	5.86	26.3	6.35	2.10	6.45	1.17	6.29	1.22	3.14	0.45	2.75	0.41	1.79	2.51
PL02-W90-1	68.7	10.6	24.6	3.57	16.4	4.50	1.52	5.27	0.99	5.79	1.22	3.36	0.52	3.29	0.51	1.45	1.48
PL02-W90-2	65.2	7.63	17.8	2.61	12.5	3.57	1.28	4.53	0.86	5.14	1.11	2.99	0.46	2.91	0.45	1.32	1.33

[a]All samples were chosen as indicated in Table 3. See *Harpp* [1995] for details.

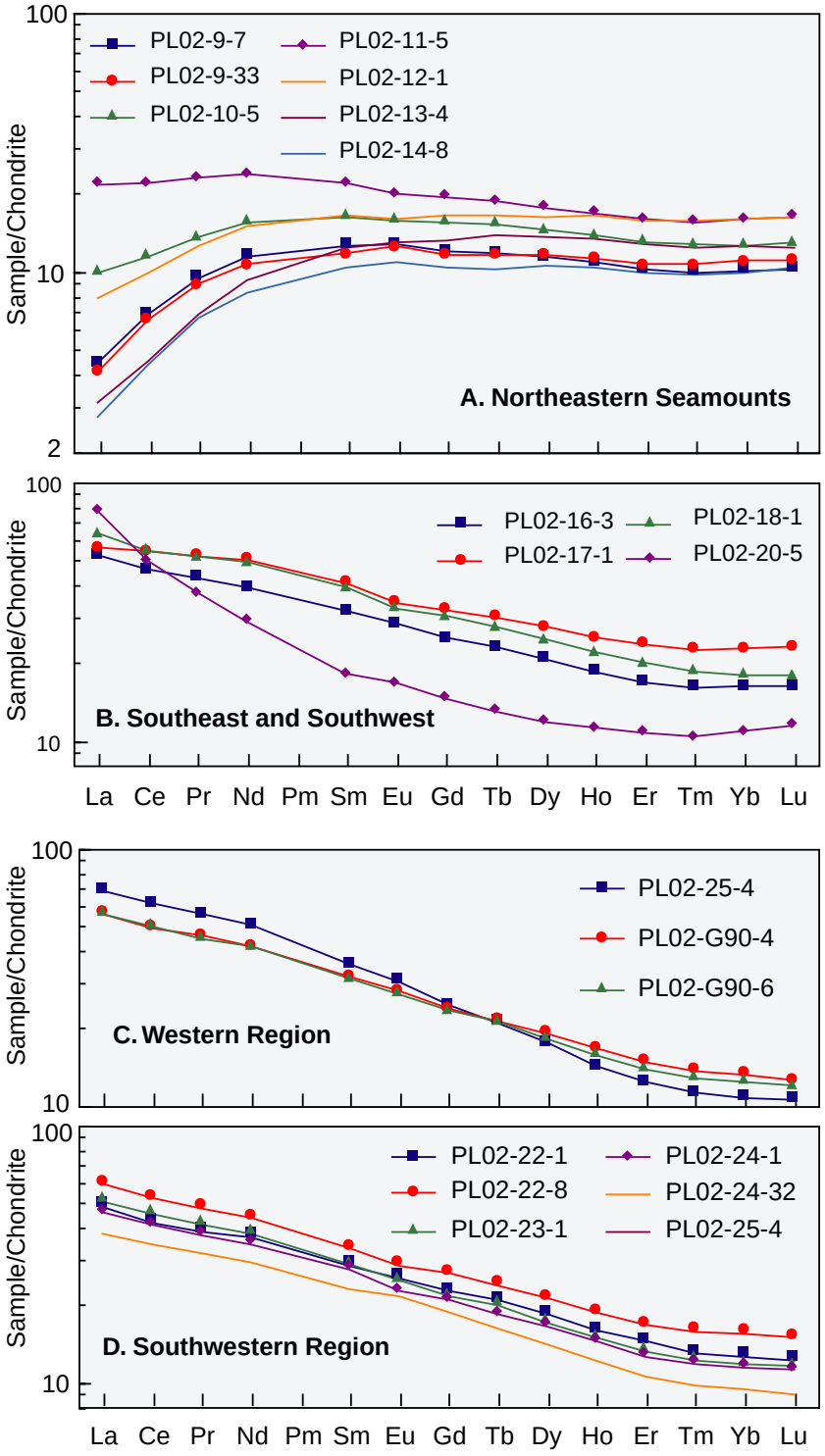

Figure 5. PLUM02 rare earth element variations by region. Concentrations are normalized to chondrite (modified from *Nakamura et al.* [1989]). (a) Northeast; (b) Southeast and southwest; (c) West; (d) Southwest.

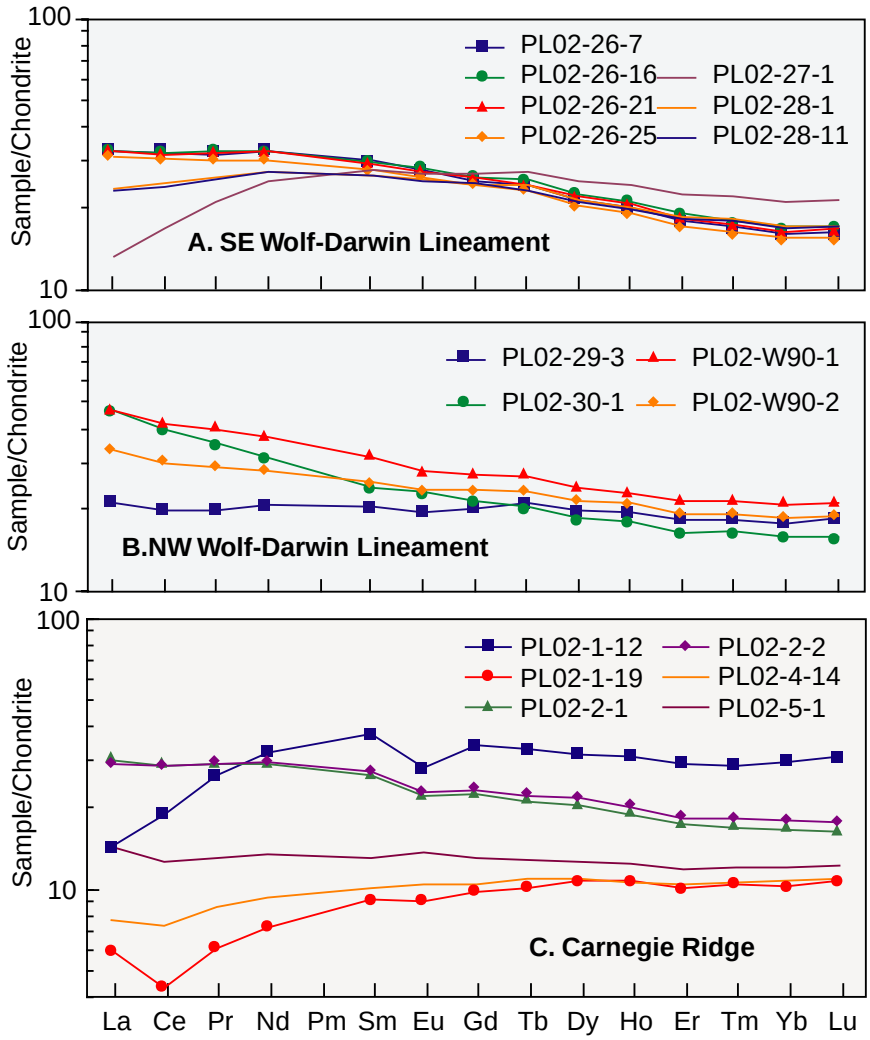

Figure 6. PLUM02 rare earth element variations by region. (a) Southeast end of Wolf-Darwin Lineament; (b) Northwest end of Wolf-Darwin Lineament; (c) Carnegie Ridge.

some ocean island volcanoes [e.g., *Davidson and Bohrson*, 1998], assimilation does not appear to influence significantly Sr, Nd, Pb, Hf, or O isotope ratios in the evolution of the Galápagos Islands [*White et al.*, 1993; *Geist et al.*, 1998; J. Blichert-Toft and W. M. White, Hf isotope geochemistry of the Galápagos Islands, submitted to *Geochemistry, Geophysics, Geosystems*, 2000, hereinafter referred to as Blichert-Toft and White, submitted manuscript, 2000]. Initial geochemical studies of the Galápagos region invoked plume-asthenosphere mixing to explain the isotopic variability in the archipelago and the adjacent Galápagos Spreading Center [e.g., *Schilling et al.*, 1982]. Such binary mixing is, however, inadequate to explain these variations. This is evident, for example, in Pb-Pb isotope plots (Figure 3), where the data clearly do not define a linear array. Three-dimensional views of the data (Animation 1 available at http://www.g-cubed.org/publicationsfinal/articles/2000GC000137/

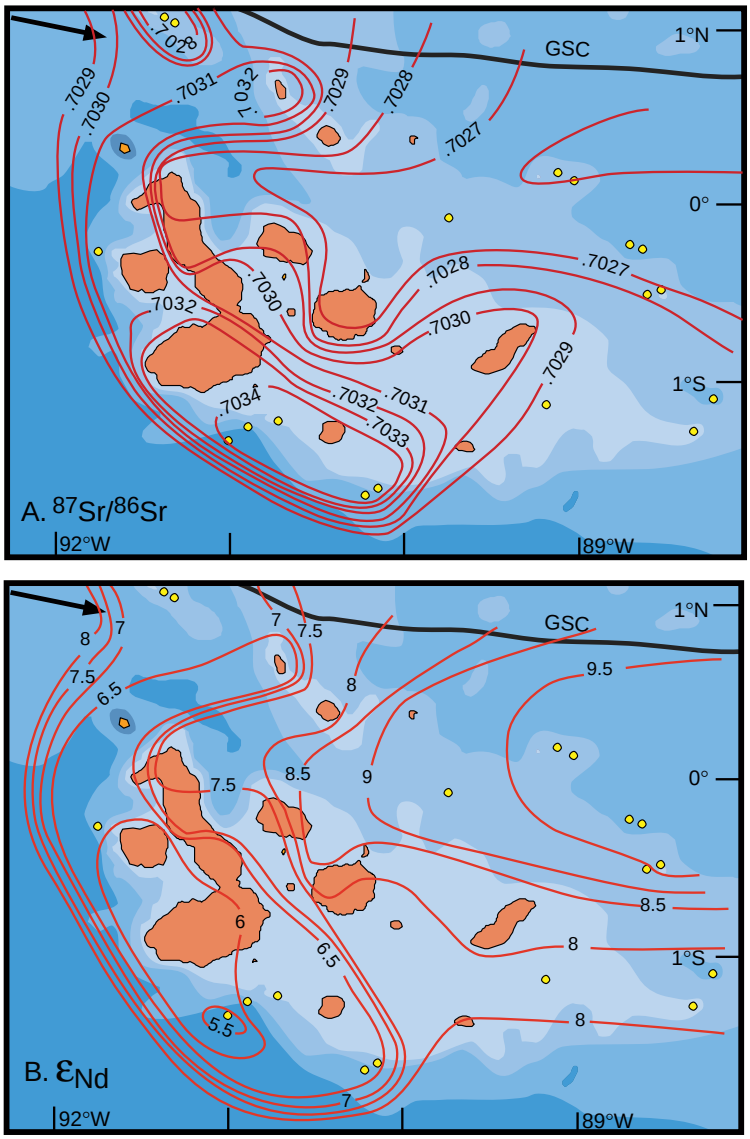

Figure 7. Geographic variation patterns for isotopic and trace element ratios. (a) $^{87}Sr/^{86}Sr$; (b) ε_{Nd}. We used average data from each site, including all the dredges and individual volcanoes from this study and from *White et al.* [1993]; the standard deviation in the average from a given site is always significantly less than variation between sites. We assumed that normal unenriched oceanic crust bounds the platform to the east and south; data from the Galápagos Spreading Center axis were used for the northern boundary constraints [*Schilling et al.*, 1982; *Verma and Schilling*, 1982; *Verma et al.*, 1983]. Locations were backtracked to their original eruption sites according to plate motion vectors from *Gripp and Gordon* [1990] and ages from *Sinton et al.* [1996] and *White et al.* [1993]. The islands and seamounts of the Wolf-Darwin Lineament (all <1 Ma) could not be corrected for plate motion because they lie "upstream" of the hot spot center. Lavas older than 5 Ma were not included in the contours (see section 5). Where islands exhibit a range in ages, separate backtracked locations were calculated (e.g., Santa Fe, San Cristobal, Floreana, Santa Cruz) [*White et al.*, 1993]. When we discuss dredge or island locations in the remainder of this work, we are referring to these age-corrected positions, unless otherwise stated. Santa Fe and Pinta have anomalously enriched signatures even in zero-age lavas [*White et al.*, 1993]. The black arrow is plate motion [*Gripp and Gordon*, 1990].

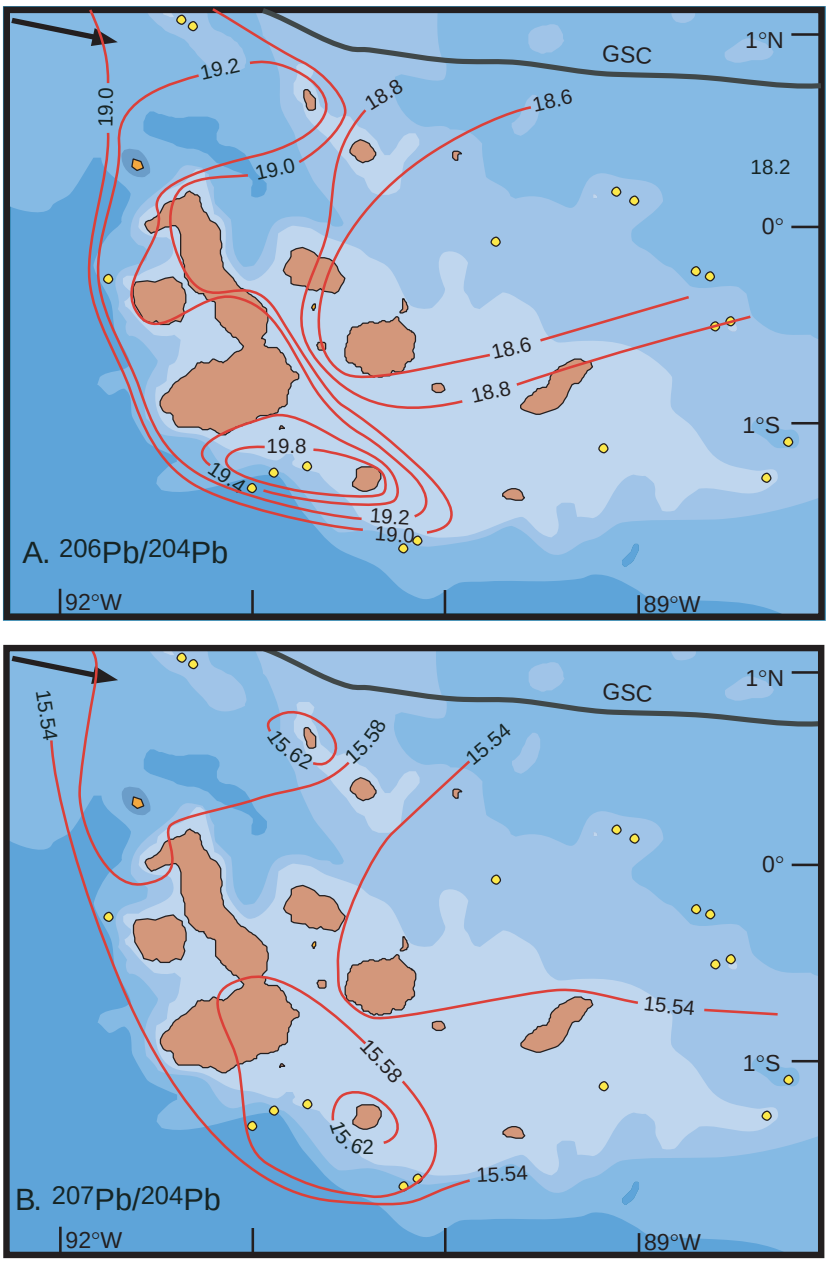

Figure 8. Geographic variation patterns for isotopic and trace element ratios. (a) $^{206}Pb/^{204}Pb$; (b) $^{207}Pb/^{204}Pb$. See Figure 7 for details.

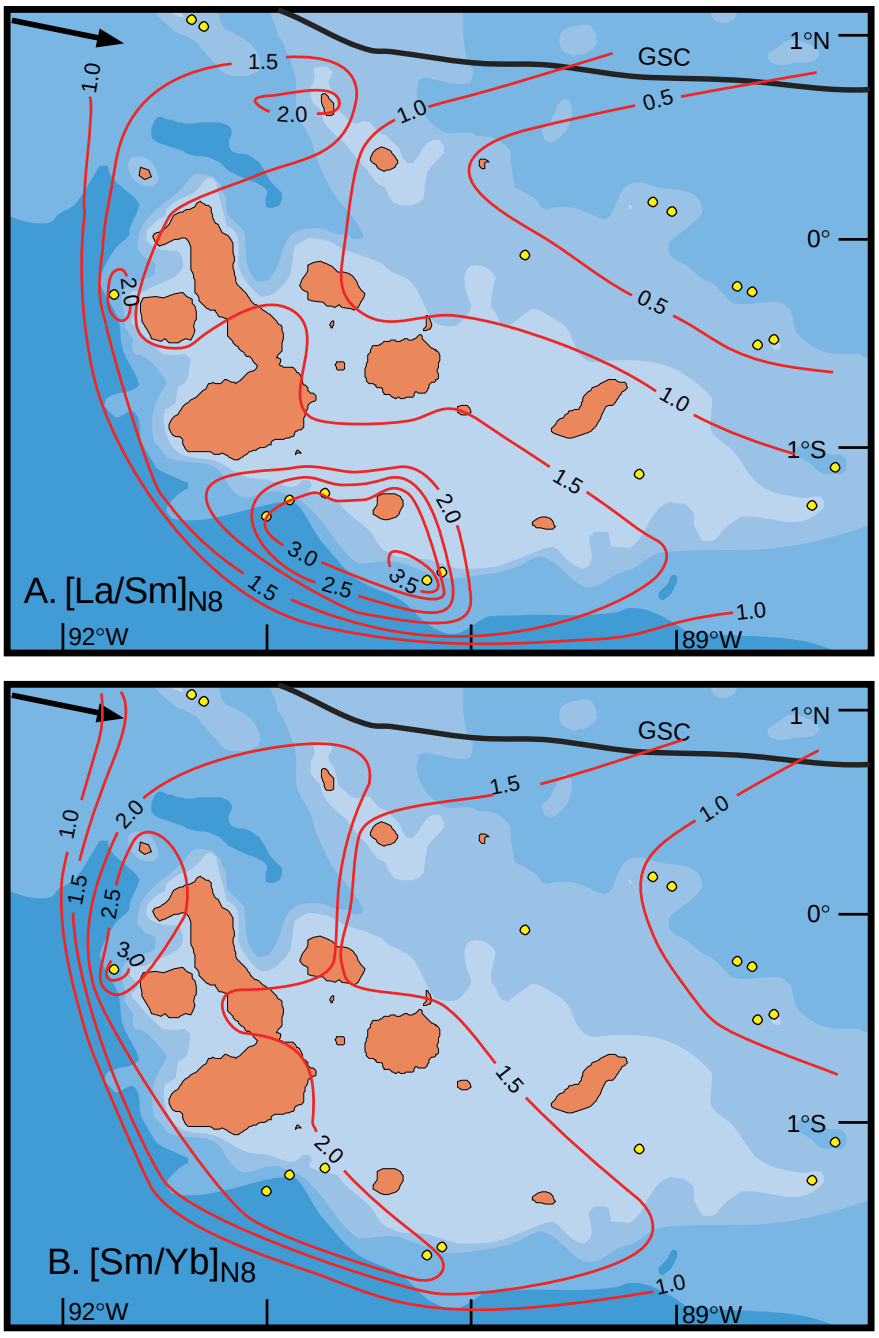

Figure 9. Geographic variation patterns for isotopic and trace element ratios. (a) La_8/Sm_{8n}; (b) Sm_8/Yb_8. See Figure 7 for details.

2000GC000137-al.mov) confirm this conclusion; the most enriched samples, including Floreana and other lavas from the southern margin, form a distinct field extending obliquely away from the main football-shaped array formed by the rest of the data.

[18] *Geist et al.* [1988] described a plume that was isotopically heterogeneous to explain the geochemical variations. With the acquisition of more isotopic data, *White et al.* [1993] proposed that the Galápagos mantle plume is internally heterogeneous, with the northern limb being compositionally distinct from the southern one. For example, Pinta exhibits lower $^{87}Sr/^{86}Sr$ and $^{206}Pb/^{204}Pb$ than Floreana lavas for the same range in ε_{Nd}. Similarly, the northern islands of Marchena, Wolf, and Darwin fall along the low ε_{Nd} side of the $^{87}Sr/^{86}Sr$-ε_{Nd} array, whereas the southern island of San Cristobal defines the high extreme [see *White et al.*, 1993, Figure 6]. This is somewhat analogous to Hawaii, where two geographic trends, "Loa" and "Kea," exhibit subtle but distinct differences in isotopic composition that have persisted over millions of years [e.g., *Stille et al.*, 1986; *Kurz et al.*, 1995].

[19] The picture is further complicated by helium isotope ratios. *Graham et al.* [1993] and *Kurz and Geist* [1999] detected the highest $^{3}He/^{4}He$ in lavas from the westernmost island of Fernandina. They argued that the "purest" plume material was therefore located beneath this area. Fernandina, however, exhibits only intermediate isotopic compositions. Instead, the most radiogenic Sr, Nd, and Pb samples are from the SW near Floreana, and they possess lower He isotope ratios. In the view of *Graham et al.* [1993] this could result either from predominately primitive, undegassed plume entraining recycled material or a plume consisting primarily of recycled material entraining undegassed material during ascent. In contrast, *Kurz and Geist* [1999] attributed the aberrant behavior of the helium isotopes to segregation of He from Sr, Nd, and Pb by partial melting.

4.2. Principal Component Analysis

4.2.1. How many end-members?

[20] The Galápagos data are consistent in a broad sense with multicomponent mixing, but the number and composition of distinct mantle reservoirs contributing to the plume remain unclear. We performed principal component analysis (PCA) on the complete Galápagos data set to establish the number of distinct end-members involved [e.g., *LeMaitre*, 1982; *Zindler et al.*, 1982; *Staudigel et al.*, 1984; *Hart et al.*, 1992a].

[21] PCA is a multivariate statistical technique commonly used to reduce the complexity of high-dimensional data. The original set of variables is transformed into a new coordinate system, using a variance-covariance matrix. The new axes are orthonormal, unique to the data set, and designed to identify the directions of greatest and least variability in the data set. The principal component vectors representing each axis correspond to different linear combinations of the variables, in this case, Sr, Nd, He, and three Pb isotope ratios. A vector that has a large eigenvalue, or variance proportion, represents a direction in the data with large variance. By choosing to consider only the vectors that represent maximum spread in the data, the system is reduced to a more manageable number of dimensions. In essence, PCA provides an alternative system for examining the data, without making any assumptions about or changes to the original variables [*Marriott*, 1974].

[22] How the variance is distributed across the principal component axes determines the number of variables necessary to describe the data set. When most of the variance is represented by only the first principal component vector, then the data can be described with minimal loss of

Table 5. Principal Component Analysis: Principal Component Analysis Results for the Entire Data Set Considering $^{87}Sr/^{86}Sr$, ε_{Nd}, $^{206}Pb/^{204}Pb$, $^{207}Pb/^{204}Pb$, and $^{208}Pb/^{204}Pb$ (n = 127)

	Variance Proportion				
Eigen Vectors	V1	V2	V3	V4	V5
Percent of total	84.7	9.6	3.3	2.1	0.3
$^{87}Sr/^{86}Sr$	−0.435	0.474	−0.693	−0.325	0.016
ε_{Nd}	0.433	−0.498	−0.710	0.214	0.126
$^{206}Pb/^{204}Pb$	−0.470	−0.063	−0.104	0.736	−0.471
$^{207}Pb/^{204}Pb$	−0.419	−0.691	0.023	−0.511	−0.293
$^{208}Pb/^{204}Pb$	−0.477	−0.216	0.070	0.213	0.822

information in one-dimensional space by two end-members. If the variance is spread over the first two vectors, then a third end-member is required to reproduce the variation in the data, and so forth.

[23] Because the relative variations in the Sr, Nd, Pb, and He isotopic ratios differ by orders of magnitude, we normalized each of these isotope ratios prior to PCA (e.g., subtract the mean of all $^{87}Sr/^{86}Sr$ measurements from each observation, then divide the difference by the standard deviation of all $^{87}Sr/^{86}Sr$ values). This process ensures that equivalent magnitudes of variation for all geochemical parameters are given equal weight [*LeMaitre*, 1982].

[24] For the comprehensive Sr, Nd, and Pb Galápagos data set, which includes data from *White et al.* [1993], *Graham et al.* [1993], *Kurz and Geist* [1999], and the PLUM02 results reported here, a principal component analysis of Sr, Nd, and Pb isotope ratios shows that 94.3% of the variance in the system is accounted for by the first and second vectors (Table 5; n = 127). The bulk of the variance is described by only the first principal component (84.7%). We know that the 9.6% attributed to the second vector must be significant in light of the discussion above, in which it was determined that binary mixing cannot be the sole process at work in the archipelago. We also believe that the 3.3% variance associated with the third vector is significant because, as discussed in section 4.2.2, this vector is necessary to describe fully the distribution of geochemical variations.

[25] When He isotope data [*Graham et al.*, 1993; *Kurz and Geist*, 1999] are included with Sr, Nd, and Pb isotope ratios, the distribution of variance between the first two vectors shifts significantly (Table 6). The first vector describes 70.9% of the variance, the second

Table 6. Principal Component Analysis: Principal Component Analysis Results for the Entire Data Set Considering $^{87}Sr/^{86}Sr$, ε_{Nd}, $^{206}Pb/^{204}Pb$, $^{207}Pb/^{204}Pb$, $^{208}Pb/^{204}Pb$, and $^{3}He/^{4}He$ (n = 36)

	Variance Proportion					
Eigen Vectors	V1	V2	V3	V4	V5	V6
Percent of total	70.9	20.6	5.5	1.7	1.1	0.2
$^{87}Sr/^{86}Sr$	−0.435	−0.281	0.313	0.795	0.030	−0.013
ε_{Nd}	0.439	0.258	−0.399	0.510	−0.564	0.059
$^{206}Pb/^{204}Pb$	−0.467	0.154	0.130	−0.236	−0.651	−0.511
$^{207}Pb/^{204}Pb$	−0.328	0.612	−0.428	0.183	0.462	−0.297
$^{208}Pb/^{204}Pb$	−0.452	0.311	−0.028	−0.106	−0.200	0.804
$^{3}He/^{4}He$	−0.297	−0.599	−0.737	−0.082	−0.056	0.014

increases to 20.6% and the third accounts for 5.5%. This suggests that He variation could be particularly important in one or more of the end-members. Results that include helium, however, should be examined with some caution, because they are based on a limited data set (n = 36): selected PLUM02 He analyzes from *Graham et al.* [1993] and lavas predominantly from the western Galápagos from *Kurz and Geist* [1999]. Furthermore, He isotopic variations could reflect factors other than mantle heterogeneity (e.g., preferential degassing of the least radiogenic He as suggested by *Graham et al.* [1993]). Even without consideration of He isotopes, however, it appears from our statistical analysis that at least three distinct mantle reservoirs are interacting to produce the geochemical variations observed in Galápagos lavas.

4.2.2. Three or four end-members?

[26] The question of whether the third vector is significant is an important one; it distinguishes between the need for three or four end-member compositions to explain Galápagos geochemical variations. The error involved in isotopic measurements is low, well under the 3–5% attributed to the third principal component vector. In fact, the magnitude of the analytical variance relative to the total variance in the data set is considerably less than 1% for all isotopic measurements except $^{207}Pb/^{204}Pb$, which is less than 3.4%, and $^{143}Nd/^{144}Nd$, less than 1.7% (analytical variance/total variance). Moreover, the full PCA for all Sr, Nd, Pb, and He isotopes yields fourth, fifth, and sixth vectors that account for 1.7, 1.1, and 0.2% of the total variance, respectively. This total of 3.0% certainly encompasses analytical uncertainty, leaving the third vector as a potential indicator of a fourth mixing end-member. In a similar application of PCA to samples from Loihi seamount, *Staudigel et al.* [1984] attributed a similar fraction of the variance (5%) to analytical uncertainty.

[27] More convincingly, the need for a fourth distinct mixing component is apparent in the Pb-Pb variation diagrams (Figure 3). Here, the data roughly form a quadrilateral. Mixing lines in Pb-Pb space are straight; the observed isotopic variations cannot be explained by only three end-members without neglecting a significant portion of the data or using extreme isotopic values that are unlike any natural samples. With addition of a fourth end-member, however, all the data can be described.

[28] At Loihi Seamount, *Staudigel et al.* [1984] found that when considering only Sr, Nd, and Pb isotopes, most of the variance could be attributed to two vectors, equivalent to three distinct mixing components. Upon consideration of helium isotopes, a third vector was needed to describe the variance. They proposed that He might therefore be decoupled from the Sr, Nd, and Pb isotopic systems. In the Galápagos data set, however, even without the addition of He, the variance requires three principal component vectors or four end-members. The importance of a second vector is only enhanced upon addition of He, not dependent on its consideration (Table 6). This observation suggests that the third and fourth end-members are not simply defined by distinct $^{3}He/^{4}He$ compositions but can be distinguished from the other two extrema by virtue of their Sr, Nd, and Pb isotopic signatures as well. Finally, new Hf isotope data reported by Blichert-Toft and White (submitted manuscript, 2000), when combined with Sr, Nd, and Pb isotope ratios, also suggest the existence of four components. We conclude therefore that four distinct mantle components contribute to Galápagos magmatism.

4.3. What Are the End-Member Compositions?

[29] To address the characteristics of the four end-members, the Galápagos data set was plot-

ted in principal component space, using the first three principal component vectors as axes. We chose four sample compositions that represent the most extreme points in PCA space that approximate a tetrahedron around the main body of the data: Floreana (FL-3), the northeast seamounts (PL02-9-7), the Wolf-Darwin Lineament (PL02-26-7), and the western region near Fernandina (PL02-25-4). That these four points originate from different regions within the archipelago lends credence to the hypothesis of four-component mixing.

[30] We calculated mixing lines among the four isotopic compositions using the isotopic and trace element data from each sample [*Langmuir et al.*, 1978]. Even though the mixing fields encompass most of the archipelago data, coverage is inadequate. To improve the situation, we adjusted the isotopic compositions of the possible end-members in an iterative fashion, looking for good coverage, logical trends, and most importantly, consistency in sample interrelationships (e.g., samples from the same volcano). The final four isotopic compositions, when mixed in varying proportions (Table 5), reproduce virtually all of the Galápagos data, as illustrated by the calculated mixing lines (Figures 10 and 11).

[31] The principal components have compositions characteristic of four regions: (1) MORB-like Sr, Nd, and Pb ratios and $^{3}He/^{4}He$, similar to the northeast seamounts; (2) enriched Sr, Nd, and Pb signatures, with $^{3}He/^{4}He$ ratios lower than MORB, similar but not identical to Floreana lavas; (3) moderately enriched Sr, Nd, and Pb, with high $^{3}He/^{4}He$, like the western edge of the hot spot; and (4) moderately enriched Sr and Nd, MORB-like $^{3}He/^{4}He$, but elevated $^{207}Pb/^{204}Pb$ and $^{208}Pb/^{204}Pb$ for a given $^{206}Pb/^{204}Pb$, similar to Wolf-Darwin Lineament lavas. Trace element concentrations for each end-member are based on each regional average.

4.4. Correspondence of End-Member Compositions to Mantle Components

[32] How do the four end-member compositions relate to the mantle, how are they distributed in the mantle, and how do they correspond to the "depleted" and "enriched" end-members originally identified by previous Galápagos studies (Table 7)?

4.4.1. Depleted end-member

[33] The mantle surrounding the plume has consistently been called upon as the source of the depleted material in Galápagos mixing models [e.g., *White et al.*, 1993]. The most depleted end-member composition falls squarely in the Pacific MORB isotopic and trace element ratio fields. We conclude, as do Blichert-Toft and White (submitted manuscript, 2000), that it is, in fact, the depleted upper mantle source of N-MORB and refer to it hereafter as DUM. In contrast, *Hoernle et al.* [2000] consider the depleted end-member to be a component of the plume itself, a perspective we believe is unsupported by geographic observations (e.g., Blichert-Toft and White, submitted manuscript, 2000).

4.4.2. "Plume" end-member

[34] Because we are no longer considering a simple binary system in the Galápagos, the concept of the "plume" or the "enriched end-member" becomes more complex. Of the three remaining components, the one that predominates in the central western Galápagos (e.g., Fernandina) is most widespread throughout the archipelago. Perhaps significantly, it is dominant in the center of the archipelago, whereas the remaining two contribute largely at the periphery. Therefore we assign this component the name PLUME. Several additional lines of reasoning suggest this component resembling western lavas represents the most pristine Galápagos plume. The current understanding of the

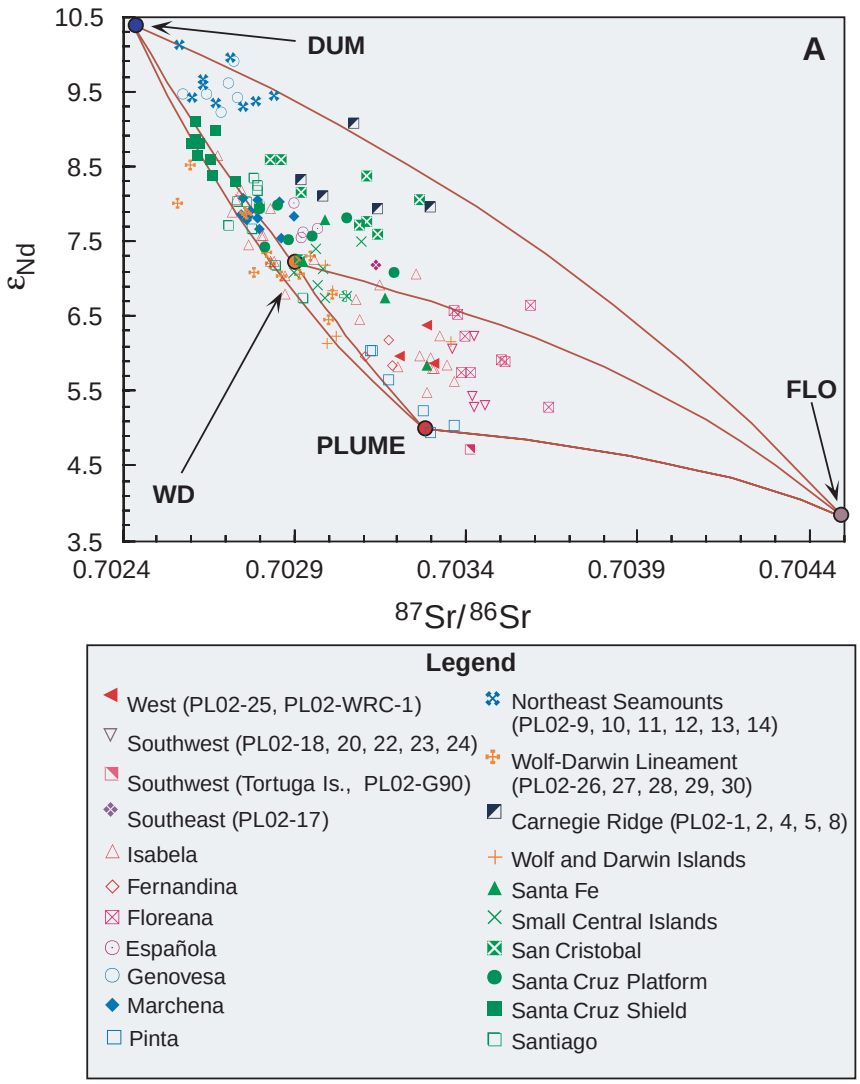

Figure 10. Selected mixing lines using FLO, PLUME, DUM, and WD compositions from Table 5. Legend for Figures 11 and 12 included; $^{87}Sr/^{86}Sr$ versus ε_{Nd}.

conventional hot spot model as it applies to the Galápagos has the main body of the plume located at the western edge of the platform, near Fernandina [e.g., *White et al.*, 1993]. Furthermore, primordial helium isotope ratios are considered a strong indication of relatively undegassed, primitive material with deep mantle origins. The highest $^{3}He/^{4}He$ ratios in the Galápagos are observed in lavas from and near Fernandina [*Graham et al.*, 1993; *Kurz and Geist*, 1999], suggesting that the young lavas erupted in the westernmost reaches of the archipelago probably represent relatively undiluted and undegassed plume material.

4.4.3. Floreana end-member

[35] Having assigned two of the four mixing compositions to the plume and surrounding asthenosphere, the nature of the remaining

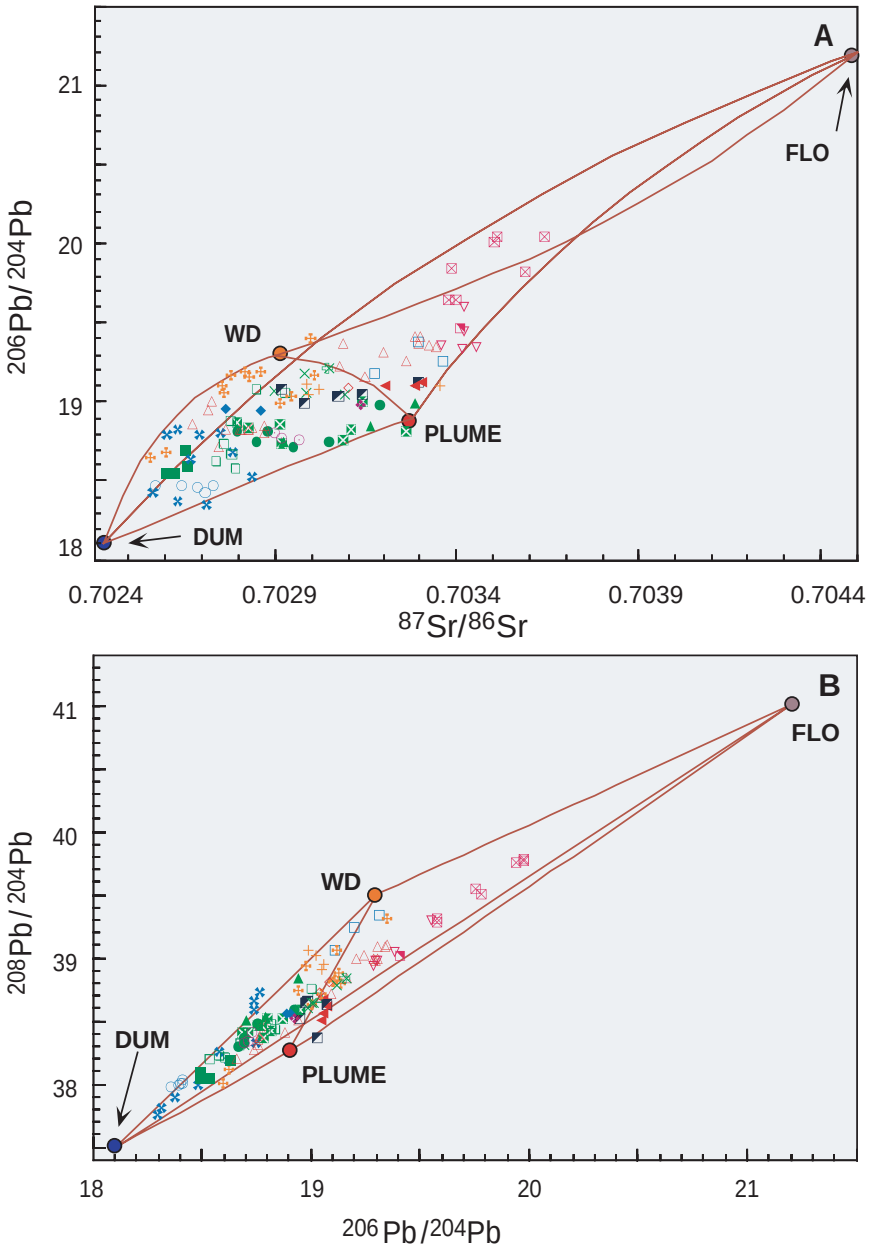

Figure 11. Selected mixing lines using FLO, PLUME, DUM, and WD compositions from Table 5. See legend in Figure 10 for symbols. (a) $^{206}Pb/^{204}Pb$ versus $^{87}Sr/^{86}Sr$; (b) $^{208}Pb/^{204}Pb$ versus $^{206}Pb/^{204}Pb$.

components is not obvious. The most enriched end-member defines the extreme in the mixing relationships and is based on Floreana lavas (now referred to as FLO). *Graham et al.* [1993] propose Floreana-like compositions as a potential mixing end-member in the Galápagos region as well.

[36] The $^{3}He/^{4}He$ ratio of FLO has to be lower than MORB to satisfy the mixing requirements

Table 7. Proposed Galápagos Mantle End-Member Compositions

	$^{87}Sr/^{86}Sr$	$^{143}Nd/^{144}Nd$	ε_{Nd}	$^{206}Pb/^{204}Pb$	$^{207}Pb/^{204}Pb$	$^{208}Pb/^{204}Pb$	$^{3}He/^{4}He$	Ba/La	La_n/Sm_n
FLO	0.70450	0.51283	3.8	21.2	15.77	41.0	3	35	8.0
PLUME	0.70328	0.51289	5.0	18.9	15.49	38.3	32	5	1.3
WD	0.70290	0.51301	7.2	19.3	15.67	39.5	9	8	0.9
DGM	0.70243	0.51317	10.4	18.1	15.46	37.5	8	1	0.1

($\sim$3 R_A). Such a helium signature is characteristic of material recycled during subduction because the material has been outgassed twice: once when originally erupted and again during the subduction process [*Kurz et al.*, 1982a; *Staudacher and Allègre*, 1988; *Farley et al.*, 1992]. Comparable signatures (enriched radiogenic isotopes but $^{3}He/^{4}He < 7–9$ R_A) have been observed at other hot spot systems including St. Helena, Tristan da Cunha, and Sao Miguel [e.g., *Kurz et al.*, 1982b; *Graham et al.*, 1992].

[37] The FLO end-member is also notable for elevated incompatible trace element (ITE) ratios such as $La/Sm_{(n)}$ and $Ba/La_{(n)}$. *Bow and Geist* [1992] observed elevated ITE ratios in most Floreana lavas, with $La/Sm_{(n)}$ extending to values greater than 10 in some main series samples. To produce the elevated ITE ratios, the mantle source must be enriched in LREE relative to chondritic levels. This observation contradicts positive ε_{Nd} values that indicate a time-averaged LREE depletion. *Bow and Geist* [1992] suggest the asthenosphere underlying Floreana has been affected by reaction with LREE-enriched, volatile-rich fluids or small degree melts ($\leq$1%) [e.g., *McKenzie*, 1989; *Hawkesworth et al.*, 1984] via metasomatism so recently that new radiogenic ^{143}Nd has not had time to accumulate (<270 Ma). Mantle metasomatism has been invoked in many ocean island settings to explain a variety of geochemical observations [e.g., *Menzies and Murthy*, 1980b; *Roden et al.*, 1984; *Dupuy et al.*, 1993; *Sen et al.*, 1993]. Blichert-Toft and White (submitted manuscript, 2000) noted the distinct high ε_{Hf}–low ε_{Nd} of Floreana lavas and their similarity in this respect to Hawaiian lavas, where both Hf-Nd and Hf-Pb isotope systematics strongly suggest the presence of recycled sediment in the source (Blichert-Toft and White, submitted manuscript, 2000).

[38] Several additional pieces of evidence support mantle metasomatism in the Floreana region: (1) elevated levels of Ba and La (as well as Rb, Sr, Th, and Pb) in the southwestern lavas compared to other Galápagos samples [*Bailey*, 1982]; (2) a break in the slope that falls consistently at 1–2 ppm Th on Th-Sr, Th-Rb, and Th-K_2O variation diagrams, indicative of residual phlogopite in the source, a typical metasomatic replacement mineral [*Bow and Geist*, 1992]; (3) the distinct convex-upward or spoon-shaped rare earth element patterns of some Floreana and PL02-20 samples indicative of residual clinopyroxene, as well as an absence of garnet in the source [*Sen et al.*, 1993]. This suggests high modal clinopyroxene in the source, another common metasomatic replacement mineral [*Bailey*, 1982]. Finally, the eruptive style of Floreana provides additional evidence for metasomatism, albeit circumstantial. Many eruptions on Floreana have been explosive, pyroclastic events; moreover, Floreana is known for producing the most alkaline lavas in the archipelago [*Bow and Geist*, 1992]. This in turn suggests the magmas have a high water content. Metasomatism has been invoked as the precursor to alkaline magmatism [e.g., *Wass and Rogers*, 1980; *Menzies and Murthy*, 1980a; *Bailey*, 1982], resulting in elevated volatile contents, and the consequently explosive nature of volcanism.

[39] The possible metasomatic origin of FLO is consistent with the recycled origin suggested by the isotopic ratios. The process of subduction involves the movement of volatile-rich fluids through the slab, a metasomatic event in its own right [e.g., *Sun and McDonough*, 1989]. On the basis of the isotopic, trace element, and morphologic evidence, we propose that the FLO component is mantle enriched in incompatible elements, which has been incorporated into the Galápagos plume relatively recently (<270 Ma). On the basis of the additional evidence described above [e.g., *Bow and Geist*, 1992], FLO may be volatile-rich with possible recycled origins.

[40] Rather than attribute the unique geochemical signature of southwestern lavas to a distinct mantle end-member such as FLO, *Kurz and Geist* [1999] invoke preferential extraction of helium from the plume as a mechanism to generate the distinctive geochemical signature observed near Floreana, as well as some of the Isabela volcanoes. They propose that the extreme incompatibility of helium in the plume causes helium to be removed from upwelling material in the immediate vicinity of Fernandina. Subsequently, plume material migrates along plate motion direction and lithospheric topography toward Floreana, where it erupts with appropriately depleted helium contents. While this model explains the regional pattern of helium isotopic variations, it does not adequately account for the other radiogenic isotope and incompatible element contents of southwestern lavas. Simple migration of the plume from Fernandina toward Floreana over ~60 km cannot result in enrichment of Sr, Nd, and Pb isotope ratios, a significant increase in ITE concentrations, nor explosive volcanism. Furthermore, Hf isotope ratios of Floreana lavas (when considered with other radiogenic isotope ratios) are particularly distinctive (Blichert-Toft and White, submitted manuscript, 2000). Consequently, we maintain that a distinct additional mantle composition, localized in the southwestern region, is required to explain the geochemical observations.

4.4.4. The fourth end-member, WD

[41] The origin of the fourth end-member, WD, is elusive because it accounts for a relatively small amount of the total isotopic variation (3.3%). It is intermediate to the other end-members in terms of $^{87}Sr/^{86}Sr$, ε_{Nd}, and $^{206}Pb/^{204}Pb$, but unique because of elevated $^{207}Pb/^{204}Pb$ and $^{208}Pb/^{204}Pb$ for a given $^{206}Pb/^{204}Pb$. WD resembles the Pinta end-member invoked by D. Christie (personal communication, 2000) as one of the components involved in the 95.5°W propagating rift lavas.

[42] WD falls along the high $^{207}Pb/^{204}Pb$ and $^{208}Pb/^{204}Pb$ trend, also observed in lavas from ocean island groups including Gough, Kerguelen, Bouvet, and St. Paul, that runs sub-parallel to the MORB array [*Dupré and Allègre*, 1983; *Hart*, 1984; *Hawkesworth et al.*, 1987]. The anomaly is characterized by relatively high Rb/Sr, $^{235}U/Pb$, and Th/U ratios that must have originated early in Earth history, through possible mechanisms such as (1) subduction of sediments into the mantle with subsequent incorporation into the OIB source [*Dupré and Allègre*, 1983], (2) reinjection of subducted oceanic crust into the OIB source [*Hart*, 1984], (3) delamination of ancient subcontinental lithosphere [*Hart*, 1984], or (4) mantle heterogeneities in the early Earth related to formation of the continents [*Hart*, 1984]. Regardless of its exact origin, the Pb isotopic signature of WD must be the result of long-lived mantle heterogeneity.

4.5. Mixing Relationships in the Galápagos Archipelago

[43] The Galápagos data do not conform to clean, single-mixing lines between pairs of end-members but are broadly consistent with

four-component mixing (Figures 10 and 11). The scatter may be attributable to variable Sr, Nd, Pb, and He concentrations within each source, and/or complex source mixtures, and/or segregation of the elements by partial melting. With only a few exceptions, most of the Galápagos data can be described by various combinations of the four end-member compositions. There is more scatter in the trace element ratios than in the isotopes, probably the result of fractionation processes during melting and fractional crystallization [e.g., *White et al.*, 1993].

[44] Given that FLO and DUM bracket the more intermediate compositions of the WD and PLUME end-members, we cannot ascertain unique mixing relationships or unravel the individual contributions of each component; often, several combinations of end-members could feasibly yield a particular composition. Instead, below we describe the first-order relationships among the Galápagos samples and the four mixing components which, however simplified, illustrate the large-scale mantle processes at work in the hot spot region (Figures 10 and 11): (1) Westernmost lavas most closely resemble the PLUME end-member, with some contribution from WD and DUM. (2) Lavas from southern Isabela volcanoes, Floreana, Tortuga, and PL02-20 through 24 are intermediate between FLO and PLUME, with minor DUM contribution. (3) The central islands may involve all four end-members. In general, however, most of the central island lavas fall in the DUM-PLUME-WD field, which is particularly evident in the Pb isotopic variations. Small contributions of FLO cannot be discounted; in the $^{87}Sr/^{86}Sr$-ε_{Nd} variation diagram (Figure 10), contributions from FLO are distinctly manifested as an offset from the DUM-WD-PLUME trend toward higher $^{87}Sr/^{86}Sr$ values. Lavas from the southern islands of San Cristobal, Española, and Santa Fe, as well as the Carnegie Ridge are all controlled to a greater extent by FLO than other sites. (4) Most Wolf-Darwin Lineament samples appear to follow a DUM-WD mixing line. Contribution of WD is manifested as a displacement in the Pb-Pb trend oblique to the main body of the data, toward high $^{207}Pb/^{204}Pb$ and $^{208}Pb/^{204}Pb$. (5) The depleted northeast seamounts and Genovesa are dominated by DUM; some islands in the north (e.g., Marchena) contain a minor PLUME contribution.

[45] In general, the regional trends elucidated from end-member mixing calculations are remarkably consistent with results from the regional principal component analysis. Where mixing appears to be largely binary, the geochemical variance is dominated by a single eigenvector, and where mixing may involve up to four end-members, variance is described by up to three eigenvectors (see Table A2 for regional PCA results). This observation is consistent with geochemical variability at individual volcanoes, which is considerably less than regional trends [e.g., *Geist*, 1992].

4.6. Refinement of the End-Members Via Melt Modeling

[46] If the four new end-member compositions are indeed more appropriate than the binary mixing model to explain geochemical variations in the Galápagos, they must also be consistent with melting systematics throughout the region. We have significantly modified the original binary melting model of *White et al.* [1993] to test the proposed end-members as a mechanism for generating the variable Galápagos lava compositions. Furthermore, this approach lets us refine the trace element composition of the end-members.

[47] Garnet strongly fractionates the heavy rare earths from the light REE during melting at depths greater than ~60–80 km [*McKenzie and O'Nions*, 1991]; material melted in the presence of garnet will exhibit high Sm/Yb

ratios for a given La/Sm. Melting in the spinel field (~25–60 km) [*McKenzie and O'Nions*, 1991], in contrast, yields a high La/Sm for a given Sm/Yb because in the absence of garnet, clinopyroxene will dominate the bulk partition coefficient.

[48] *White et al.* [1993] calculated total melt compositions in the garnet and spinel fields of the enriched and depleted end-members; they used constant clinopyroxene-REE partition coefficients [*Hart and Dunn*, 1992] and assumed equilibrium melt processes. In our modified melt model, we assume a polybaric, equilibrium melting process (see Figure 12 for details).

[49] Using the refined melting model, we first tested the straightforward hypothesis of two-component plume-MORB mixing in the Galápagos. We chose G90-4, Tortuga Island, as the enriched end-member and PL02-9-33, a northeast seamount, as the depleted one (Figure 12, top). Superimposed on the calculated melting model are the fractionation-corrected $La_8/Sm_{8(n)}$ and $Sm_8/Yb_{8(n)}$ data from the combined island and dredge data set (the fractionation correction algorithm is described in the caption to Table A1). Despite our modifications of the binary melt model, the southern Galápagos data plot below the field of melts that is calculated from this binary mixture, even in the spinel stability field. Thus it is not possible to generate the La/Sm and Sm/Yb ratios of the southern samples with a simply binary source mixture, even under a variety of melting conditions. The failure of the model is predictable because the isotopic variations require more than two sources and that isotopic variability is caused in turn by long-term fractionation of trace elements.

[50] Instead, we turn to the four end-member compositions dictated by isotopic constraints, DUM, PLUME, FLO, and WD. The depleted mantle meets the isotopic and trace element requirements of DUM. PLUME has a more enriched composition, possibly close to primitive mantle (PM). Yet PM, with ε_{Nd} ~0, is too isotopically enriched for PLUME. We estimate that PLUME has primitive mantle-like trace element compositions ($La/Sm_{(n)}$, $Sm/Yb_{(n)}$ ~1), but the isotopic signature of PLUME ε_{Nd} ~ 5. Even under this assumption, an extremely small, shallow degree melt of PLUME only can reproduce La/Sm ratios of the least extreme Floreana lava. Heterogeneity within the plume is thus required by incompatible element concentrations and ratios as well as by isotope ratios. The Floreana-inspired source composition used for mixing calculations consists of a small degree MORB melt (0.1%) generated in the spinel melting field combined with primitive mantle (98.9% of the source) for a final ε_{Nd} of ~3.8.

4.6.1. Regional variations in source composition

[51] To determine the specific end-member combinations responsible for each Galápagos subregion, we have taken into account the change in mineralogy (garnet > ~60 km; spinel ~25–60 km) with depth and integrated it with a polybaric melting model [e.g., *McKenzie*, 1985]. The mineralogy appropriate to each depth is used to calculate iteratively incremental melt compositions.

[52] Initially, we determine the relative proportions of DUM and PLUME necessary to produce the observed range in ε_{Nd} of the samples. Using our polybaric model, we then generate melts at a variety of initial depths. If none of these melt compositions reproduces the data, we then add FLO to the initial source composition, adjusting the relative DUM and PLUME contributions such that the final ε_{Nd} values match those of the samples, then repeat the melting process. Usually several combinations of end-members can successfully generate most

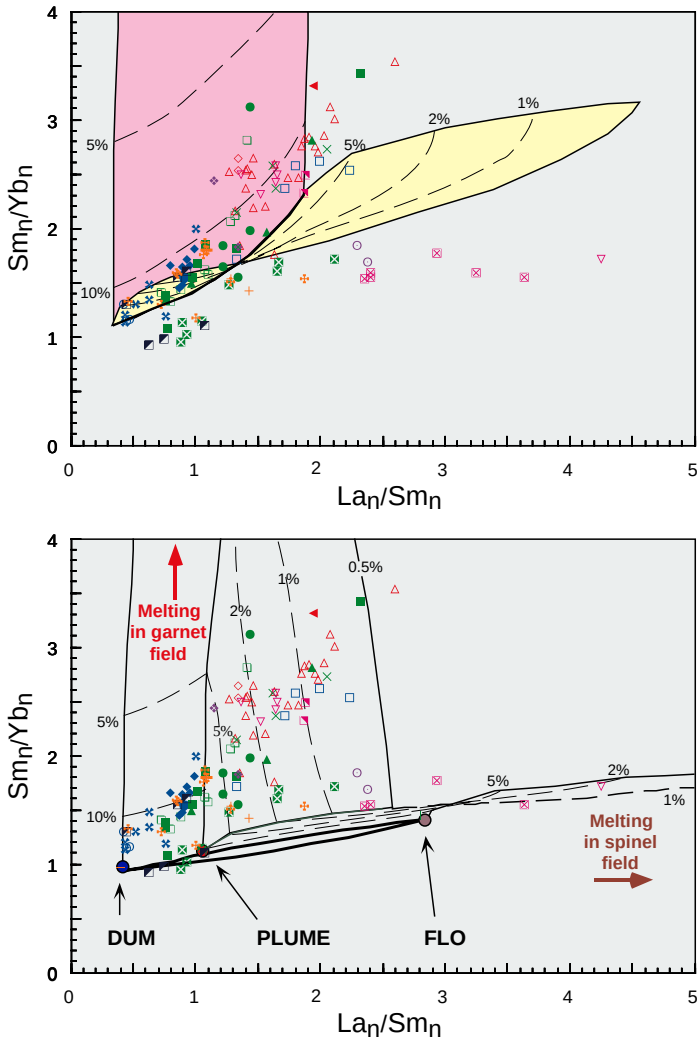

Figure 12. (top) Polybaric melts of enriched-depleted end-members in the spirit of *White et al.* [1993]. An ascending parcel of mantle is melted a small degree for every increment of upwelling. The liquid is partially extracted and pooled, and the remaining residue is used as the source for the next increment of melting. The composition of the aggregate melt reflects the average pressure and temperature of the entire melting interval [*O'Hara*, 1985; *Langmuir et al.*, 1992]. The actual melting process for each increment is assumed to be equilibrium melting. *Plank and Langmuir* [1992] have demonstrated that equilibrium melting closely reproduces a diverse range of complex melting mechanisms and is therefore a good approximation for any mantle melting process. We have used the *Langmuir et al.* [1992] relationship for the melt function, which averages to ~1.2% melting per kilobar upwelling but varies systematically with depth. In addition, we employed the algorithm developed by *Gallahan and Nielsen* [1992] to calculate the clinopyroxene-rare earth element partition coefficient ($D_{\text{cpx-REE}}$) for each melt composition, to account for the dependence of $D_{\text{cpx-REE}}$ on the composition of the melt, particularly the Al_2O_3 content [*Gallahan and Nielsen*, 1992]. Symbols are as follows: mixing trend between depleted (PL02-9-33) and enriched (PL02-G90-4) compositions (solid black line; see text for details); compositional changes with varying degree of melting (thin dashed lines); melting in garnet peridotite stability region (pink field); melting in spinel peridotite stability region (yellow field). (bottom) Polybaric melts of DGM (in the garnet field), PLUME (in the garnet and spinel fields), and FLO (in the spinel field). See Figure 10 legend for symbols.

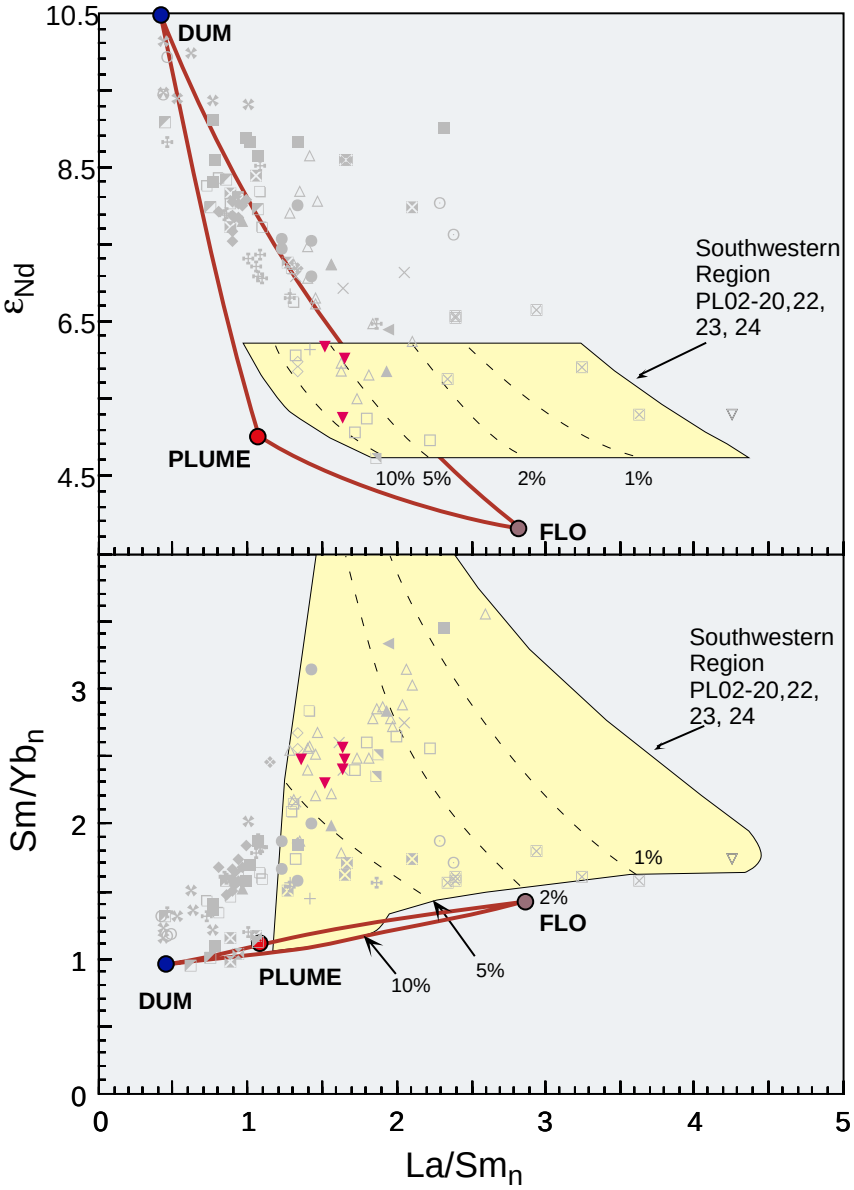

Figure 13. Polybaric melting, varying mantle mineralogy with depth, for calculated source compositions of the southwest dredges. Solid circles represent DGM, PLUME, and FLO end-member compositions. Thick solid lines indicate binary mixing between end-members. Dashed lines indicate variations in degree of melting. Fractionation correction process is described in the caption to Table A1. See Figure 10 legend for symbols and Figure 12 for additional melt model details.

Galápagos lava compositions. When faced with this difficulty, we examine the regional pattern and choose the source composition and melting conditions that most closely agree with regional patterns (Table A3). Although not unique, these solutions are first-order attempts to describe mixing and melting relationships in the Galápagos. In Figure 13, we illustrate an example of

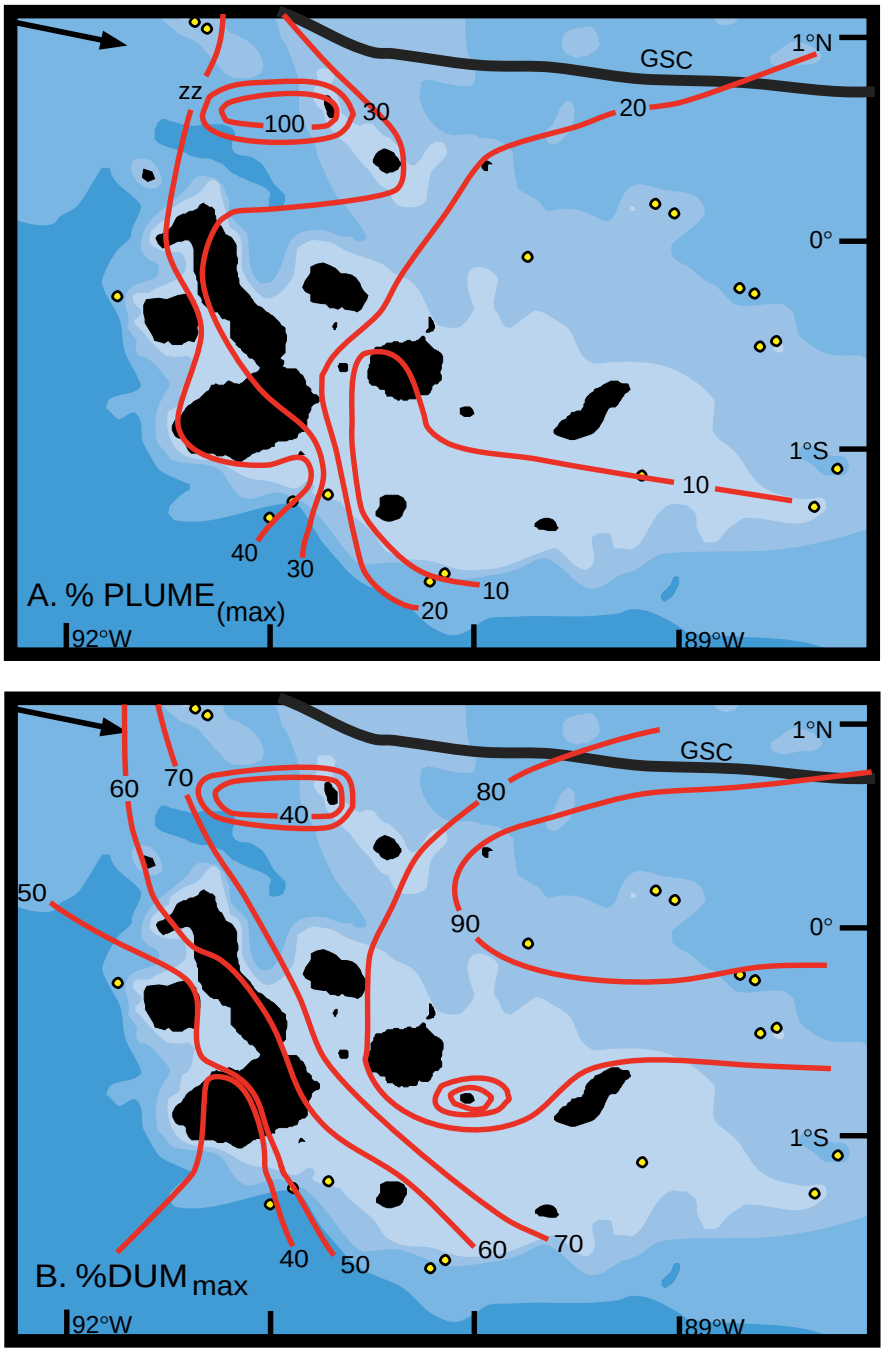

Figure 14. (a) Contours of maximum PLUME contributions from end-members to Galápagos lavas. (b) Contours of maximum DUM contributions from end-members to Galápagos lavas. (c) Contours of maximum FLO contributions from end-members to Galápagos lavas. Darker contour is limit of 2000 m bathymetry; lighter contour is limit of 1000 m bathymetry. Data from the Galápagos Spreading Center have been included as well [*Schilling et al.*, 1982; *Verma and Schilling*, 1982; *Verma et al.*, 1983].

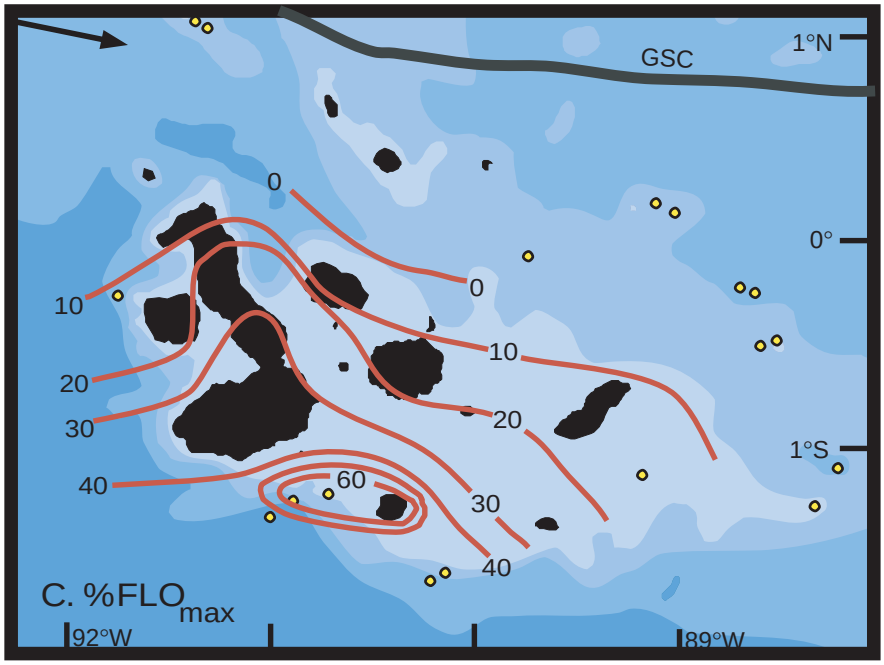

Figure 14. (continued)

these calculations for the southwest dredges based on both source composition and melting conditions.

[53] Regional trends in calculated melting and mixing systematics include the following: (1) The deepest, most extensive melting occurs in the western archipelago; PLUME is the dominant contributor, but there is an unexpectedly large contribution from DUM and a small contribution from FLO. (2) Extent of melting, PLUME, and FLO contributions decrease with distance north on Isabela, while DUM increases. (3) FLO dominates in the southwest region, with some PLUME but minimal DUM contributions. The southwest exhibits some of the most extreme melting behavior in the archipelago, with small degree melting at Floreana. (4) At the center of the archipelago, depth and extent of melting are highly variable. DUM and PLUME dominate, with only small contributions from FLO. (5) The northeast seamounts (PL02-9 through 14) exhibit a wide range in extents of melting, largely at shallow depths. DUM dominates almost completely, with only a small PLUME contribution. (6) Pinta and Marchena lavas may, on average, originate as small degree melts from slightly greater depths than the NE seamounts. Despite their proximity, the source composition of Marchena resembles the NE seamounts, while Pinta lavas require a predominantly PLUME source. This result is not in keeping with the regional pattern but is consistent with the anomalous nature of Pinta [e.g., *Kurz and Geist*, 1999]. (7) The Wolf-Darwin Lineament requires a greater PLUME contribution in the NW segment than in the SE. Low extents of melting occur at generally shallow depths across the WDL. (8) The Carnegie Ridge is strongly dominated by DUM, and melting is generally more extensive than in the central islands.

[54] It is apparent from the above that mixing occurs primarily between the various plume components (PLUME, FLO, WD) and asthenosphere (DUM). Mixing between plume components appears to be more restricted.

[55] Because source composition calculations described above are not unique, we have chosen to examine the maximum PLUME, FLO, and DUM contributions to each Galápagos lava composition; the geographic distributions of the maximum end-member contributions for PLUME, FLO, and DUM are shown in Figure 14. This approach provides the simplest interpretation of the available data, with the caveat that more complex models could be constructed from the same information. Moreover, results are consistent with our broad understanding of plume dynamics. For instance, PLUME contributions are most significant in the west, decreasing systematically to the east, as expected from the tectonic setting of the hot spot.

[56] Perhaps the most intriguing pattern is displayed by FLO, which is highly localized in the southwest corner of the platform (Figure 14). FLO contributions decrease progressively with distance from the Floreana, most notably to the north and east. This pattern is particularly well illustrated in the Isabela volcanoes.

[57] WD, the fourth end-member, is distinctive only in terms of its Pb isotopic ratios. Its influence is limited to northern lavas, including the Wolf-Darwin Lineament, Pinta, NE seamounts, and GSC. The composition of WD so closely resembles either DUM or PLUME in terms of its major and trace element contents that we cannot distinguish it in REE-based calculations.

5. Discussion

5.1. Relationship of Galápagos Array and Galápagos End-Members to Mantle Reservoirs

[58] For over the past two decades, researchers have employed isotopic ratios in ocean island basalts and MORB to determine the distribution and origin of chemical heterogeneity in the mantle. Several sets of end-members have been proposed over the years. Below we compare the four Galápagos mixing components, DUM, PLUME, FLO, and WD, to the various schemes.

[59] A widely used set of mantle reservoirs was developed by *White* [1985] and refined by *Zindler and Hart* [1986] in their review of geochemical heterogeneities in the mantle, which was later elaborated upon by *Hart* [1988]. Five mantle components were defined according to Sr, Nd, and Pb isotopic distinctions [*Zindler and Hart*, 1986] and largely correspond to White's groups: (1) DMM, the depleted MORB mantle; (2) HIMU (mantle with high U/Pb ratios, White's St. Helena); (3) EMI (enriched mantle, White's Kerguelen);(4) EMII (another enriched mantle, White's Society); and (5) PREMA (prevalent mantle, White's Hawaii).

[60] Most OIB and MORB data fall in a tetrahedron defined by the four *Zindler and Hart* [1986] end-members, DMM, HIMU, EM I, and EM II, in $^{87}Sr/^{86}Sr$-ε_{Nd}-$^{206}Pb/^{204}Pb$ space [*Hart et al.*, 1992a]. Many ocean island groups form linear arrays that have been interpreted as binary mixing between mantle reservoirs. Interestingly, most arrays do not indicate mixing between the pure mantle components. Many originate from locations along the axes rather than from a single vertex and spread out in a multitude of directions in a fan-shaped arrangement. Remarkably few arrays point toward DMM, despite the depleted mantle being the most likely candidate in mantle mixing scenarios. The Galápagos is one of the rare OIB arrays that extends directly into the MORB field.

[61] Like the majority of the global oceanic basalt data, three of the Galápagos end-members, DUM, PLUME, and WD, are contained

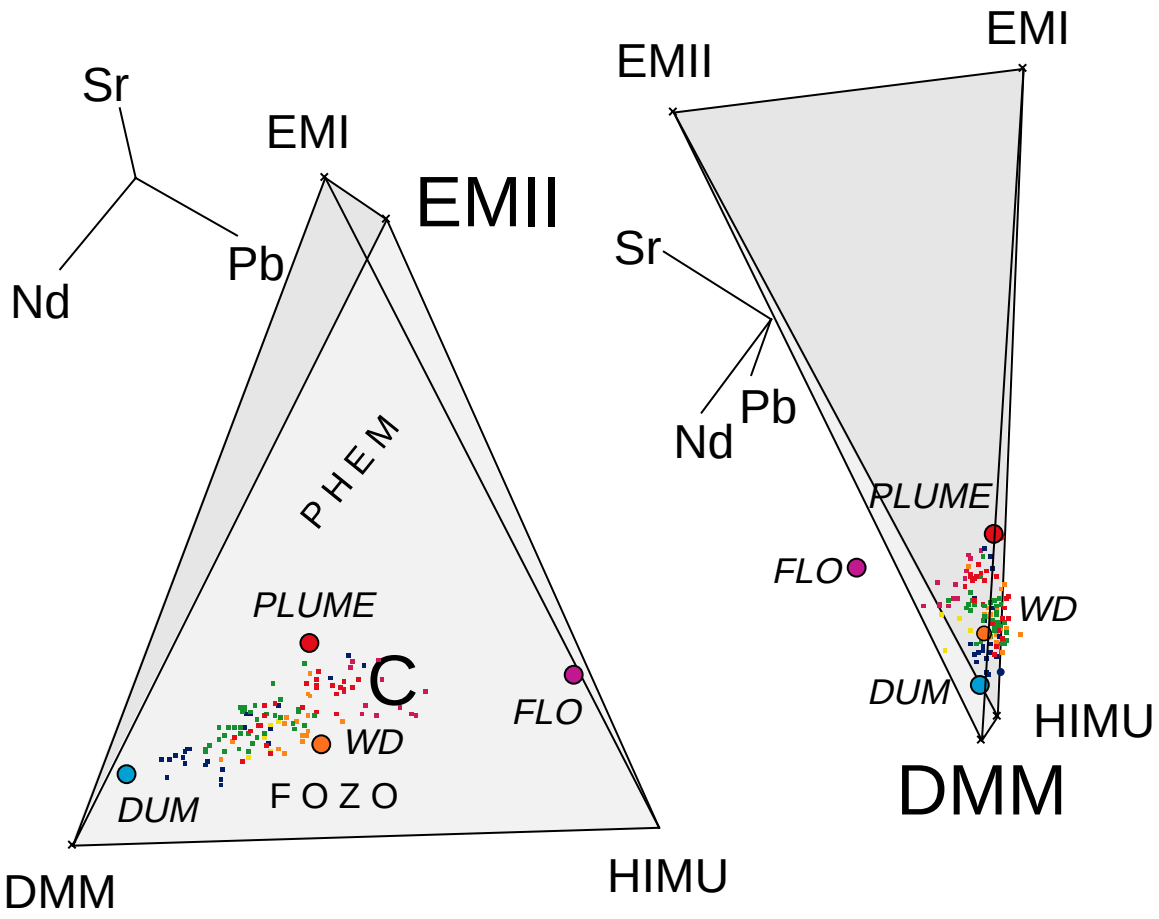

Figure 15. Tetrahedron in $^{87}Sr/^{86}Sr$, ε_{Nd}, and $^{206}Pb/^{204}Pb$ isotopic space of major mantle reservoirs [*Zindler and Hart*, 1986; *Hart et al.*, 1992a, 1992b]. Solid circles represent Galápagos mixing end-members: DGM (blue); PLUME (red); WD (orange); and FLO (pink). Galápagos data are colored by region, see legend in caption to Figure 10. On left is the view with EMII apex pointing out of the page, EMI apex into the page; DMM and HIMU line lies in the plane of the page. On the left the tetrahedron is rotated 90°; DMM points out of the page; EMI and EMII lie in the plane of the page. PHEM, **C** and FOZO represent hypothesized compositions of high $^{3}He^{4}He$ mantle end-member [*Farley et al.*, 1992; *Hanan and Graham*, 1996; *Hart et al.*, 1992a]. See text for details and Animation 1 for regional color scheme.

within the DMM-HIMU-EMI plane of the tetrahedron (Figure 15). DUM lies closest to the depleted mantle apex. None of the other end-members corresponds to the *Zindler and Hart* [1986] mantle reservoirs. PLUME is centrally located in the DMM-HIMU-EMI face, and WD sits closer to the DMM-HIMU join. The ITE-enriched end-member FLO lies outside the tetrahedron toward HIMU, off the HIMU-DUM-EMII face of the Figure 15. This is in keeping with the observation of *Zindler et al.* [1982] that metasomatically altered material will fall outside the main mantle array. The complexity of the mantle end-members required to explain Galápagos geochemical variations is consistent with emerging evidence that mantle-derived magmas may be drawing on numerous distinct lithologies, including garnet pyroxenite and eclogite [*Hirschmann and Stolper*, 1996], embedded in a peridotite

matrix. *Lassiter et al.* [2000], for example, present evidence for involvement of pyroxenite- and peridotite-derived melts of the lithospheric mantle in Hawaiian post-erosional lavas. The relationship between lithologic heterogeneity in the mantle and isotopic and trace element composition of magmas remains, however, completely unknown.

[62] A fifth mantle component may also exist, but its composition has been more difficult to define because it may lie within the tetrahedron defined by DMM, HIMU, EM I, and EM II. Several researchers have observed that the pseudo-binary mixing arrays of ocean island data tend toward a common area internal to the *Zindler and Hart* [1986] tetrahedron, and that ^{3}He/^{4}He ratios generally increase within the arrays toward this area [e.g., *Hart et al.*, 1992a; *Farley and Craig*, 1992; *Hart et al.*, 1992b; *Graham et al.*, 1993; *Hanan and Graham*, 1996]. This fifth component, which may be common to many or all plumes, has intermediate or depleted Sr, Nd, and Pb isotopic compositions and unradiogenic He (>30 R/R_A). It has been called PHEM by *Farley and Craig* [1992], "FOZO" by *Hart et al.* [1992a], and "**C**" by *Hanan and Graham* [1996]. We will use the term **C** for the remainder of this discussion, for simplicity's sake, but consider that even though they differ in detail, FOZO, PHEM, and **C** spring from the common deduction that there is a distinct mantle reservoir with high ^{3}He/^{4}He and intermediate Sr, Nd, and Pb isotope ratios. The location of the mantle reservoir is not well constrained, although there has been some speculation on this issue [e.g., *Hart et al.*, 1992a, 1992b; *Hanan and Graham*, 1996].

[63] The hypothesized compositions of FOZO, PHEM, and **C** are illustrated alongside the Galápagos data and end-members in Figure 15. PLUME falls in the region of Sr-Nd-Pb isotopic space defined by **C**. The geochemical composition assigned to the plume is not the most enriched in the archipelago. Other studies of ocean island basalts including Loihi and Samoa have yielded similar results; lavas with the highest ^{3}He^{4}He ratios (>20 R/R_A) exhibit intermediate Sr, Nd, and Pb signatures [*Kurz et al.*, 1983; *Staudigel et al.*, 1984; *Farley et al.*, 1992; *Farley and Craig*, 1992; *Hart et al.*, 1992a, 1992b; *Hilton et al.*, 2000].

[64] Most ocean island plumes appear to be mixtures of one or more of the three classical mantle plume reservoirs (HIMU, EMI, EMII) with **C**. Yet only three thus far, the Galápagos, Iceland, and Easter, clearly seem to involve "pure" **C**. The ubiquitous nature of **C** suggests that this reservoir may be a major mantle component and may constitute the principal material of most mantle plumes. The Galápagos, then, along with Iceland and the Easter Island chain, may represent extremes in the spectrum of mantle plumes in that they are sampling relatively pristine **C**. Other plumes may be incorporating HIMU, EMI, and EMII components during ascent or include more of those components originally, which then mask the original **C** signatures. The Galápagos may provide us with a rare opportunity to observe the geochemistry of a significant mantle source in relatively unpolluted form.

5.2. Melting Variations

[65] Parameters such as degree and depth of melting are only partially constrained by our calculations; nevertheless, they are useful as qualitative indicators of broad patterns, which may be summarized as follows. The western archipelago is notable for the wide range in degrees of melting, longest melting intervals, and greatest initial depths. Extent of melting generally decreases with distance from Fernandina; depths of melting increase to the east but decrease to the north and more abruptly to the south. These observations indicate that mantle temperatures in the west are highest and strongly

support the traditional hot spot model wherein the plume center is located at the "upstream" end of the island chain [*Wilson*, 1963]. The wide range in degree and extent of melting downstream from Fernandina suggests that magma supply drops off rapidly with distance from the conduit center as the plume becomes progressively depleted by melt removal.

5.3. Mantle Dynamics

5.3.1. Entrainment of depleted mantle

[66] Results of the mixing and melting models suggest that the PLUME end-member is diluted by depleted mantle, even at its center beneath Fernandina. Moreover, many of the lavas observed in the Galápagos archipelago exhibit anomalously depleted geochemical signatures, particularly for an ocean island setting. Several models have been proposed to explain the contribution of depleted material (DUM) to Galápagos lavas, most of which invoke entrainment of the upper mantle. *Geist et al.* [1988] attributed the horseshoe-like isotopic pattern in the Galápagos to entrainment of asthenosphere into the central region of a torus formed by the head of an initiating plume [*Griffiths*, 1986]. An alternative possibility follows from the laboratory experiments of *Richards and Griffiths* [1989] that demonstrated that steady state entrainment of depleted mantle could occur if a plume is bent by shear forces in the mantle caused by motion of the overlying plate. The thermal plume warms the surrounding asthenosphere, which in turn becomes buoyant; rising asthenosphere is then trapped in the horizontal part of the bent plume. This results in entrained depleted mantle in the central part of the tilted conduit, surrounded by swaths of enriched plume along the borders. In the case of the Galápagos, the enriched material is concentrated in E-W trending bands at the northern and southern limits of the bent part of the plume, with depleted material at the center of the archipelago [*White et al.*, 1993].

[67] Numerical modeling of *Bercovici and Lin* [1996] suggests yet another possibility. They found that "gravity currents" deform the plume into a torus, or mushroom shape, as a consequence of cooling of plume top by overlying lithosphere. Consequently, this leads to concentration of the plume chemical signature in a circle around the edge of the plume. Asthenosphere will be drawn upward under the mushroom head. Both the rise and conductive heating by the plume contribute to melting of this asthenosphere. If the surrounding mantle is static, the expected geochemical pattern is a ring of "enriched" isotopic signatures surrounding more "depleted" ones. If the lithosphere and uppermost asthenosphere are moving, however, this pattern may be deformed into the horseshoe shape seen in the Galápagos [e.g., *Ribe and Christensen*, 1994]. The mixing and melting systematics in Galápagos are compatible with both this scenario and the bent plume/thermal entrainment model of *Richards and Griffiths* [1989].

5.3.2. Entrainment of FLO?

[68] It is not clear whether FLO is part of the "pristine" plume or whether it is an exotic component entrained during ascent or incorporated in the upper mantle. The evidence from this study only supports the conclusion that FLO is an enriched source with metasomatic characteristics, localized in the southwest corner of the Galápagos. Either FLO has not been associated with the plume long enough to be thoroughly mixed into the main body, or else convection within the plume is not vigorous enough to homogenize its different components. A speculative explanation is that the rising plume encountered a small pocket of altered subducted crust embedded in the upper mantle [e.g., *McKenzie*, 1985, 1989], affecting only the southern portion of the plume. It is possible that this heterogeneity will be short-

lived and that this part of the hot spot will eventually revert to more typical plume signatures once FLO has been exhausted. In contrast, *Hoernle et al.* [2000] observe spatial geochemical zonation in 14.5 Ma lavas collected in a transect across the Galápagos hot spot trace (Cocos Ridge) off the coast of Costa Rica which may correspond to the variations observed in the present-day archipelago. *Hoernle et al.* [2000] attribute these variations to steady state plume heterogeneity; alternatively these observations could imply long-lived heterogeneous regions in the mantle (not originally related to the hot spot) with which the plume has been interacting throughout its history.

5.3.3. Mantle currents

[69] Regardless of whether the plume conduit is actually being bent by asthenospheric currents and the dragging lithosphere, enriched material appears to be present throughout the mantle beneath the Galápagos. The progressive decrease in PLUME contribution eastward (Figure 14) intimates an asthenospheric current in the direction of plate motion, pulling mantle material downstream, perhaps insufficient to bend the entire conduit, but strong enough to encourage entrainment of depleted mantle downstream of the plume center (Figures 16 and 17). Most convincingly, the highly localized FLO component may be spreading eastward, becoming progressively diluted in the process.

[70] Mantle material is not only moving "downstream" (i.e., in the direction of plate motion) but also northward toward the GSC. First, we know that plume material influences the composition of lavas erupted along the GSC [e.g., *Schilling et al.*, 1982]. Furthermore, the FLO contours are displaced toward the GSC; this is particularly well illustrated in the volcanoes of Isabela (Figure 14). The global *S* wave velocity model by *Zhang and Tanimoto* [1992] records low velocity zones beneath ridges that are elongated and deepen toward adjacent hot spots. The extension of the low velocity zone between the hot spot and the ridge occurs between 100 and almost 300 km depth for the St. Helena-Southern Mid-Atlantic Ridge system [*Zhang and Tanimoto*, 1992]. This may be the mechanism whereby plume is transported to the GSC to be incorporated into the upwelling system that feeds the ridge. It is possible then that this ridgeward flow may occur everywhere along the GSC but is only observable where the plume induces additional melting north of the Galápagos Archipelago (Figure 17). Moreover, the GSC is migrating northeast relative to the hot spot, at almost 50 mm yr^{-1} [*Wilson and Hey*, 1995]. This may be an additional explanation for the migration of plume material northward and its incorporation into the GSC [e.g., *Verma et al.*, 1982, 1983; *Schilling*, 1991].

[71] Does plume material flow through an "asthenospheric channel" to a single point on the ridge (most likely 92°N, where the most "enriched" isotopic signatures occur) from which it is then distributed along axis (perhaps as melt) [e.g., *Morgan*, 1978; *Schilling et al.*, 1982], or is there a much broader flow from the plume toward the GSC, with perhaps each ridge segment being supplied independently? Two primary observations favor the latter. First, new data from the GSC show that the isotopic "peak" along the GSC, so often invoked in channelized flow models [e.g., *Schilling et al.*, 1982], is in fact a broad, multihundred kilometer region where plume-influenced MORB is erupted, not a single point of enrichment (J.-G. Schilling and R. H. Kingsley, personal communication, 2000). Moreover, the isotopic gradients continue smoothly across the transform fault at 90°50′W. Second, geochemical signatures of near-axis Galápagos seamounts and islands mimic the enrichment pattern along strike of

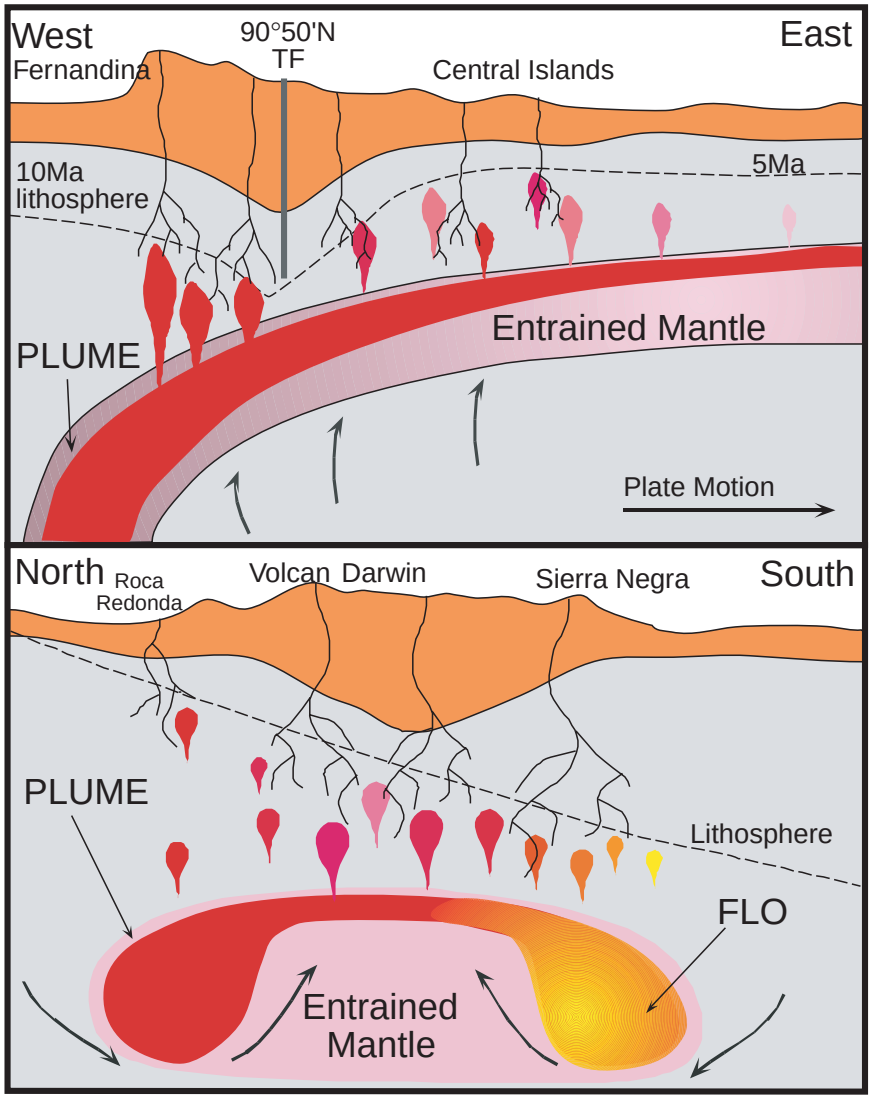

Figure 16. Pictures of Galápagos plume, not drawn to scale. Red represents PLUME, yellow represents FLO, gray is surrounding depleted mantle, and pink is entrained depleted mantle. Color gradations represent mixing among the various components. Dashed line represents thickness of lithosphere [from *Feighner and Richards*, 1995a, 1995b]. Arrows mark entrainment of depleted asthenosphere. (top) West-east cross-section through center of archipelago. Color of melt diapir represents mixture of components (e.g., red is mostly PLUME, yellow is mostly FLO, pink is a mixture of depleted mantle and PLUME, etc.). Bent configuration of the plume is illustrated here, with accompanying asthenospheric entrainment. Depletion of melts generally increases to the east but is variable beneath the central islands. Melting is deeper and more extensive in the west. FLO is not shown in this diagram. (bottom) North-south cross-section from Roca Redonda to Sierra Negra, along Isabela, in the bent part of the plume (i.e., main conduit is farther west in this figure). Note that depleted mantle is being entrained into the center of the plume, and FLO is localized in the south.

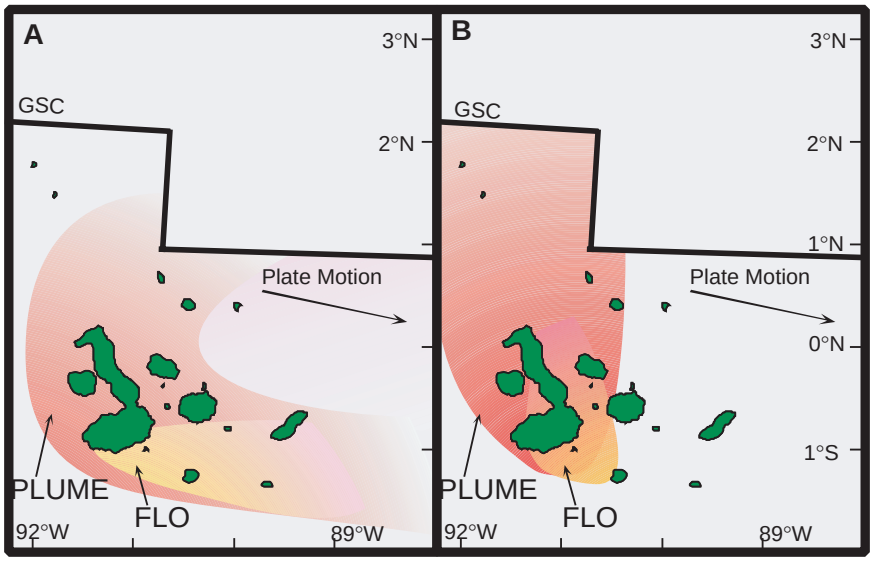

Figure 17. Pictures of Galápagos plume, not drawn to scale. Color scheme is same as in Figure 16. (a) Map view of the Galápagos plume, at shallow mantle levels. Flow of plume is eastward, in the direction of plate motion. Note the distribution of concentrated (brightest red) plume in a horseshoe-like pattern, with depleted (grayer) material at the center. FLO is indicated in yellow and is concentrated in the southwest but mixes eastward with asthenospheric flow. (b) Map view of the Galápagos plume, at deeper mantle levels. Flow of plume is toward the Galápagos Spreading Center.

the ridge, only at slightly more depleted levels. This suggests the isotopic compositions of magmas erupted along the GSC simply reflect the geographic distribution of plume material longitudinally owing to an along-axis supply from the plume.

[72] The amount of entrainment of ambient mantle by an ascending plume is controversial, as is whether it occurs in the upper or lower mantle [e.g., *Hauri et al.*, 1994; *Griffiths and Richards*, 1989; *Farnetani and Richards*, 1995]. Yet by far most of the material mixing with the Galápagos plume is the depleted upper mantle. On the basis of global mixing trends, only at hot spot ridge systems does the upper mantle play such a significant role in plume dilution [e.g., *Hart*, 1992a]. We believe this phenomenon may be the direct result of the particular tectonic setting of the Galápagos plume, similar to that of the Iceland and Easter plumes. With a potentially significant portion of the plume being displaced toward the spreading center, the main conduit may be sufficiently weakened, or spread out, that dilution by surrounding asthenosphere is rendered more likely than where the plume remains intact (compare to Hawaii).

5.4. *Northern Galápagos Province*

[73] The precise relationship of the northern volcanoes, including the NE Seamounts, Marchena, Genovesa, and the WDL, to the Galápagos plume remains enigmatic [e.g., *Morgan*, 1978; *Harpp et al.*, 2000]. It is clear from our results that many of the lavas erupted in this northern province exhibit significant contributions from the depleted mantle and are geochemically similar to Pacific near-axis seamounts [*Harpp et al.*, 2000; *Allan et al.*, 1989; *Fornari et al.*, 1988]. Interestingly, these volcanoes are comparable or slightly larger in aerial extent to Pacific seamounts [*Christie et*

al., 1990]. Why are such structures only observed in the northern parts of the Galápagos archipelago? Moreover, why are seamounts more numerous immediately north of the archipelago than on flanks of the GSC far from the influence of a hot spot [e.g., *Canales et al.*, 1997]?

[74] The abundance of small volcanic structures throughout the northern Galápagos may be a manifestation of the interaction between the GSC and the plume, particularly the elevated heat flow throughout the region [e.g., *Williams et al.*, 1974]. *Epp and Smoot* [1989] have shown that near-axis seamounts in the North Atlantic are observed in greater abundance between Iceland and the Hayes fracture zone than along non–hot spot influenced segments of the Mid-Atlantic Ridge [e.g., *Schilling*, 1985]. The increased volume and frequency of volcanic activity near–hot spot influenced ridges may be the result of plume-derived heterogeneities in the underlying mantle and increased melting of asthenosphere owing to elevated mantle temperatures. Moreover, the thin lithosphere close to the ridge can be penetrated easily, increasing the likelihood that melts will reach the surface [*Epp and Smoot*, 1989; *Shen et al.*, 1993; *Phipps Morgan*, 1997]. Finally, the seafloor is anomalously shallow near the hot spot due to crustal thickening and mantle buoyancy. A structure the size of the average Pacific near-ridge seamount [e.g., *Allan et al.*, 1989], if constructed on top of this shallow ocean floor, will actually be subaerial (e.g., Genovesa, Wolf, and Darwin Islands [*Harpp et al.*, 2000]).

[75] Volcanic lineaments and fissures such as those observed on and extending from Genovesa support control of recent volcanic activity by regional stresses possibly induced by plume-ridge interactions, perhaps precursors of an impending ridge jump as the GSC attempts to remain in close proximity with the plume. Lithospheric weaknesses may channel passively derived melts to the surface, providing a window into the mantle throughout this northern province [e.g., *Hey*, 1977; *Harpp et al.*, 2000].

[76] An additional mechanism that may explain the prevalence and orientation of volcanic structures north of the main archipelago was proposed by *Small* [1995], in a study of plume-ridge interaction in the Southern Ocean. He suggests that aseismic ridges, observed not only in the Galápagos (i.e., the Wolf-Darwin Lineament) but also at hot spot-ridge systems around the world, may be the surficial manifestation of plume flow toward the spreading center as the ridge migrates over the plume center. Plume material ascends toward the ridge, guided by the shallowing lithospheric structure, resulting in oblique aseismic lineaments. While this model adequately explains observations at many hot spot ridge systems, it should be noted that the GSC is closer to the hot spot (within <200 km at the WDL) than those systems examined by *Small* [1995]. Moreover, the WDL is much smaller than most of the ridges examined in *Small* [1995], consisting of several discrete islands and seamounts rather than a continuous feature. Consequently, the GSC and the Galápagos hot spot may be interacting more extensively than other hot spot ridge systems, resulting in more complex dynamics than can be elucidated from our limited reconnaissance data (K. S. Harpp and D. J. Geist, manuscript in preparation, 2001).

5.5. The ~5–11 Ma Plume

[77] Tantalizing clues into the history of the Galápagos plume and its relationship to the GSC are provided by the Carnegie Ridge samples (PL02-1 through PL02-10, and PL02-17). Most of the dated samples range from 5 to >11 Ma [*Sinton et al.*, 1996]. When these samples are backtracked along plate motion

vectors, their eruption sites fall close to the present-day plume center: PL02-4, 5, 8, and 17 are located off the coast of Fernandina, PL02-1 along the southern escarpment near Española, and PL02-9 and 10 east of Volcan Wolf. In every case, samples from these dredges do not fit into the contours drawn based on younger lavas but are instead consistently more depleted. It follows, then, that these Carnegie Ridge samples require more DUM in their sources per unit of PLUME to account for the depleted isotopic signatures.

[78] The Galápagos plume of ~5–11 Ma appears to differ from the recent plume in that the "older" plume incorporated a greater proportion of depleted mantle. We attribute this observation to changes in the tectonic relationship between the ridge and the hot spot. According to plate reconstructions by *Wilson and Hey* [1995], prior to ~5 Ma, for at least several million years, the GSC and the Galápagos plume were nearly superimposed, similar to the Iceland-Mid-Atlantic Ridge system today. Thus any plume material erupted in this configuration should be diluted by contributions from the depleted ridge source.

[79] Qualitative bathymetric observations support the geochemical data. *Hey* [1977] noted that the bathymetric saddle located east of the main Galápagos archipelago roughly corresponds to an increase in volcanic productivity along the Cocos Ridge. He concludes that the hot spot was located exclusively beneath the Cocos Plate during this period; the GSC must have migrated over the hot spot after this time (~12 Ma), leaving the plume beneath the Nazca plate today. The anomalously depleted 5–11 Ma lavas lie at the western edge of this saddle along the Carnegie Ridge, off the eastern limit of the main platform. They must therefore represent lavas from the transition period during which the hot spot and the GSC were superimposed, erupting lavas onto both the Cocos and Nazca Plates without forming a significant volcanic platform.

6. Conclusions

[80] Our new isotopic and trace element results from dredges across the Galápagos Platform, which double existing coverage, confirm the previously established east-facing horseshoe pattern. Depleted geochemical signatures are located at the center of the archipelago, whereas the northern, western, and southern peripheries exhibit more enriched signatures. Principal component analysis leads to the conclusion that four isotopically distinct mantle components contribute to Galápagos magmas. Three of these components may be intrinsic to the plume (PLUME, FLO, and WD); the fourth is indistinguishable from the MORB source and is presumably the shallow asthenosphere. PLUME broadly corresponds to the high $^{3}He/^{4}He$ mantle reservoir (**C**, PHEM, FOZO) proposed by several researchers [e.g., *Hart et al.*, 1992a; *Farley et al.*, 1992; *Hanan and Graham*, 1996]. The FLO component, which is the dominant influence on southern volcanoes, particularly Floreana, is the most incompatible element-enriched component. FLO has retained much of its geographic integrity and has not completely mixed with the main body of the plume; it may have existed for at least 14.5 Ma [*Hoernle et al.*, 2000]. The fourth end-member, WD, detected only in the northern islands and seamounts and in axial lavas from the GSC, is distinguishable primarily by its isotopic characteristics.

[81] The distributions of both PLUME and FLO illustrate the two primary forces at work in the mantle beneath the Galápagos. First, we observe a downstream flow related to shear in the asthenosphere caused by plate motion and ambient mantle flow, manifested as decreasing contributions of PLUME and FLO in the direction of plate motion. Second, there may be a

Table A1. Correlation Table for Galápagos Data[a]

	$^{87}Sr/^{86}Sr$	ε_{Nd}	$^{206}Pb/^{204}Pb$	$^{207}Pb/^{204}Pb$	$^{208}Pb/^{204}Pb$	Ba	La	Nd	Sm	Yb	La/Sm_n	Sm/Yb_n
$^{87}Sr/^{86}Sr$	1.000											
ε_{Nd}	−0.867	1.000										
$^{206}Pb/^{204}Pb$	0.840	−0.852	1.000									
$^{207}Pb/^{204}Pb$	0.567	−0.581	0.773	1.000								
$^{208}Pb/^{204}Pb$	0.791	−0.832	0.953	0.885	1.000							
Ba	0.720	−0.705	0.737	0.521	0.705	1.000						
La	0.703	−0.790	0.716	0.395	0.636	0.789	1.000					
Nd	0.530	−0.653	0.530	0.202	0.438	0.516	0.911	1.000				
Sm	0.425	−0.546	0.437	0.135	0.349	0.367	0.814	0.974	1.000			
Yb	−0.126	0.201	−0.123	−0.024	−0.091	−0.190	−0.005	0.204	0.365	1.000		
La/Sm_n	0.726	−0.763	0.787	0.558	0.734	0.926	0.811	0.520	0.351	−0.270	1.000	
Sm/Yb_n	0.514	−0.661	0.521	0.145	0.411	0.478	0.853	0.926	0.881	−0.095	0.501	1.000

[a]Correlation matrix for isotopic and low-pressure fractionation corrected trace element data in the entire Galápagos data set. All data used were fractionation corrected as follows. We calculated liquid lines of descent for simple fractional crystallization [*Nielsen*, 1988] at one atmosphere for a comprehensive Galápagos data set that includes (1) the PLUM02 samples, including major [*Sinton*, 1993] and trace element concentrations (this paper and *McBirney* [1993]), element data from microprobe analysis of seamount glasses [*Sinton*, 1993] and (2) the major and trace element data for subaerial samples from *White et al.* [1993]. Local compositional variations were taken into account by calculating fractionation trends for individual sites (i.e., each dredge location or volcano). This is in lieu of the method chosen by *White et al.* [1993], wherein one fractionation line is used to correct the entire data set. We chose the most primitive sample at each site as the parental melt composition, based on MgO content. We projected the data from each site along the slopes on variation plots to their predicted value at 8% MgO [*Klein and Langmuir*, 1987]. For the most part, the first crystallizing phases are plagioclase and olivine, joined later in some cases by clinopyroxene.

Table A2. Regional Principal Component Analysis Results for the Entire Galápagos Data Set, for Sr, Nd, Pb, and He Isotopic Ratios[a]

Region	Parameters Considered in Analysis						Variance Proportion, %				
	$^{87}Sr/^{86}Sr$	ε_{Nd}	$^{206}Pb/^{204}Pb$	$^{207}Pb/^{204}Pb$	$^{208}Pb/^{204}Pb$	$^{3}He/^{4}He$	e_1	e_2	e_3	e_4	E_5
WDL-NE	X	X	X	X	X	X	82.4	10.8	6.0	0.5	0.2
	X	X	X	X	X		80.7	11.4	7.2	0.6	0.0
WDL	X	X	X	X	X	X	79.6	13.2	5.0	1.9	0.3
	X	X	X	X	X		82.0	11.9	3.7	2.0	0.4
W-SW-SE	X	X	X			X	60.9	25.7	13.3	0.1	0.0
	X	X	X	X	X		85.3	11.6	2.3	0.6	0.1
SW-SE	X	X	X	X	X		89.5	8.6	1.6	0.3	0.0
NE	X	X	X			X	72.0	20.4	4.6	0.0	0.0
	X	X	X	X	X		88.3	9.8	1.3	0.6	0.1
Central Diff.	X	X	X	X	X		89.5	6.0	3.2	1.3	0.1
Central	X	X	X	X	X		79.9	9.5	6.1	4.1	0.4
Region	Parameters Considered in Analysis						Variance Proportion, %				
	$^{87}Sr/^{86}Sr$	ε_{Nd}	$^{206}Pb/^{204}Pb$	$^{207}Pb/^{204}Pb$	$^{208}Pb/^{204}Pb$	$^{3}He/^{4}He$	e_1	e_2	e_3	e_4	e_5
NE Smts.	X	X	X	X	X		67.1	27.4	4.0	1.5	0.0
WDL	X	X	X	X	X		82.3	12.0	3.2	2.0	0.4
	X	X	X	X	X	X	79.6	13.2	5.0	1.9	0.3
West	X	X	X	X	X		83.4	13.9	2.0	0.5	0.2
	X	X	X	X	X	X	74.3	17.9	6.6	0.7	0.5
SW	X	X	X	X	X		64.5	22.5	11.2	1.8	0.1
	X	X	X	X	X	X	74.4	20.5	3.7	1.1	0.3
Central Diff.	X	X	X	X	X		87.3	8.3	2.8	1.5	0.1
Central	X	X	X	X	X		79.0	11.4	5.7	3.5	0.3
Marchena, Genovesa, NE Smts.	X	X	X	X	X		66.7	25.7	6.2	1.3	0.1
Carnegie Ridge	X	X	X	X	X		54.8	26.3	17.4	1.5	0.0

[a]Symbols are as follows: e_1, e_2, etc. represent eigenvalues. Only the variance proportion attributable to each eigenvalue is shown. Regions are as follows: NE, northeast seamounts (PL02-9 through 14); WDL, Wolf-Darwin Lineament (PL02-26 through 30, Wolf and Darwin Islands); W, west (PL02-25, WRC, Fernandina, Isabela); SW, southwest (Floreana, PL02-20 through 24); SE, southeast (PL02-5, 17, Española); Central Diff., central islands with differentiated rocks, Santiago, Rabida, Pinzon, Santa Cruz and Volcan Alcedo; Central, all central islands.

Table A3. Proportions of Sources and Melting Conditions for Galápagos Lavas[a]

Region	Islands	Dredges (PL02-)	Range in Melting, %	Most Depleted Composition					Most Enriched Composition				
				Melting in Garnet, %	FLO	DUM	PLUME	ε_{Nd}	Melting in Garnet, %	FLO	DUM	PLUME	ε_{Nd}
West	Fernandina	25, WRC	2.5 to 9	9.0	0.106	0.447	0.447	6.3	3.0	0.178	0.329	0.493	5.8
West	V. Wolf, V. Darwin		VD 4 to 6 VW 2.5 to 5	3.5	0.082	0.826	0.092	8.6	3.5	0.200	0.560	0.240	6.7
West	Volcan Alcedo		6 to 9	5.0	0.140	0.602	0.258	7.0	3.5	0.309	0.415	0.276	5.9
West	Volcan Sierra Negra		5 to 10	6.5	0.290	0.355	0.355	5.7	6.5	0.389	0.306	0.306	5.4
West	Volcan Cerro Azul		4 to >10	6.5	0.307	0.485	0.208	6.2	2.0	0.364	0.382	0.254	5.7
Southwest		18, 20, 22, 23, 24	1 to 10	9.0	0.151	0.425	0.425	6.2	0.0	0.463	0.054	0.483	4.7
Southwest	Floreana		1 to 5	0.0	0.353	0.582	0.065	6.6	0.5	0.620	0.342	0.038	5.2
Southeast	Espanola		1 to 3	0.0	0.166	0.751	0.083	7.9	0.5	0.219	0.703	0.078	7.5
Central/SE	San Cristobal		1 to >10	0.5	0.000	0.800	0.200	8.5	0.5	0.189	0.649	0.162	7.2
Central	Santiago		SE 1 to >10 NW 3 to 6	3.5	0.026	0.779	0.195	8.3	1.0	0.000	0.500	0.500	6.7
Central	Santa Cruz Shield		1 to >10	2.5	0.039	0.865	0.096	9.0	0.5	0.129	0.784	0.087	8.2
Central	Santa Cruz Platform		4 to >10	2.5	0.082	0.734	0.184	7.9	3.5	0.222	0.622	0.156	7.0
Central	Santa Fe		3 to >5	3.5	0.012	0.692	0.296	7.7	3.5	0.290	0.355	0.355	5.7
North	Pinta		1 to 4	2.0	0.000	0.324	0.676	6.0	0.5	0.000	0.000	1.000	5.0
North	Marchena		4 to 5	2.5	0.000	0.762	0.238	8.2	1.5	0.000	0.657	0.343	7.5
Northeast		9 through 14	2 to >10	2.0	0.000	0.967	0.033	10.1	0.0	0.000	0.886	0.114	9.2
WDL		26, 27, 28	1 to 5	2.0	0.000	0.825	0.175	8.7	2.0	0.000	0.567	0.433	7.0
WDL	Wolf, Darwin	29, 30	2 to 5	0.5	0.000	0.605	0.395	7.2	0.0	0.000	0.364	0.636	6.1
Carnegie Ridge		1, 2, 4, 5	>10	4.0	0.000	0.860	0.140	9.0	9.0	0.180	0.738	0.082	7.8

[a]Proportions of DGM, PLUME, and FLO as well as melting conditions that successfully reproduce Galápagos data set. "Most Depleted Composition" represents the set of parameters necessary to reproduce the most depleted lava in each regional group; "Most Enriched Composition" similarly is the set of parameters that reproduces the most enriched lava for each region. Proportions of each end-member (FLO, DUM, and PLUME) are indicated in the columns; WD is not included in the calculations owing to its lack of distinction in REE composition. We emphasize that these are not unique solutions but a first order attempt to describe mixing and melting relationships in the Galápagos.

deep, strong lateral flow of mantle toward the GSC, feeding the upwelling ridge system [e.g., *Zhang and Tanimoto*, 1992]. This asthenospheric current is a potential mechanism for supplying enriched material to the spreading ridge. Superimposed on these mantle dynamics is the thermal regime, controlled locally by the plume but dominated regionally by the adjacent ridge. Temperatures decrease downstream as entrainment of the depleted mantle and distance from the plume increase.

[82] While there is significant flow from the plume to the ridge, there is little evidence that the Wolf-Darwin Lineament serves as a shallow lithospheric pipeline from the hot spot to the ridge as proposed by *Morgan* [1978]. Instead, it may be a leaky normal fault [*Feighner and Richards*, 1995a, 1995b; *Feighner and Harpp*, 1996], or magmatism induced by regional stress fields, similar to what is observed at Genovesa [*Harpp et al.*, 2000]. Magmatism is channeled along lines of existing regional stress, serving as a window into the distribution of plume and depleted mantle in the region between the plume and the ridge.

[83] Lavas erupted ~5–11 Ma from the Carnegie Ridge provide a preliminary picture of the older Galápagos hot spot and its relationship to the adjacent spreading ridge. The northward migration of the GSC relative to the Galápagos hot spot may be reflected in the anomalous depletion of the Carnegie Ridge samples relative to lavas from the main archipelago.

Acknowledgments

[84] We would like to thank Michael Cheatham for assistance with analytical procedures. Dennis Geist provided insightful comments and discussions; helpful reviews were provided by Pat Castillo, Mike Garcia, and Terry Naumann. Thanks to David Baird for technical assistance and to Dan McKenzie for guidance on modeling melting. We are also grateful to the crew and other members of the scientific party of the R/V *Thomas Washington* for their help and our scientific colleagues on PLUME-2 for stimulating discussions about the Galápagos. This work was supported by NSF awards OCE89-17031 and OCE92-03748 to WMW and CHE-9996141 to KSH.

References

Allan, J. F., R. Batiza, M. R. Perfit, D. J. Fornari, and R. O. Sack, Petrology of lavas from the Lamont seamount chain and adjacent East Pacific Rise, 10°N, *J. Petrol.*, *30*, 1245–1298, 1989.

Bailey, D. K., Mantle metasomatism- continuing chemical change within the Earth, *Nature*, *296*, 525–530, 1982.

Bercovici, D., and J. Lin, A gravity current model of cooling mantle plume heads with temperature-dependent buoyancy and viscosity, *J. Geophys. Res.*, *101*, 3291–3309, 1996.

Bow, C. S., and D. J. Geist, Geology and petrology of Floreana Island, Galápagos Archipelago, Ecuador, *J. Volcanol. Geotherm. Res.*, *52*, 83–105, 1992.

Canales, J. P., J. J. Danobeitia, R. S. Detrick, E. E. E. Hooft, R. Bartolome, and D. R. Naar, Variations in axial morphology along the Galápagos spreading center and the influence of the Galápagos hotspot, *J. Geophys. Res.*, *102*, 27,341–27,354, 1997.

Cheatham, M. M., W. F., Sangrey, and W. M. White, Sources of error in external calibration ICP-MS analysis of geological samples and an improved nonlinear drift correction procedure, *Spectrochim. Acta, Part B*, *48B*, E487–E506, 1993.

Christie, D. M., and C. Fox, Morphologic evolution of the margins of the Galápagos platform, *Eos Trans. AGU*, *71*, 1578, 1990.

Christie, D. M., R. A. Duncan, A. R. McBirney, M. A. Richards, W. M. White, and K. S. Harpp, Drowned islands downstream from the Galápagos hotspot imply extended speciation times, *Nature*, *355*, 246–248, 1992.

Davidson, J. P., and W. A. Bohrson, Shallow-level processes in ocean island magmatism: Editorial, *J. Petrol.*, *39*, 799–801, 1998.

Dupré, B., and C. J. Allègre, Pb-Sr isotope variations in Indian Ocean basalts and mixing phenomena, *Nature*, *303*, 142–146, 1983.

Dupuy, C., P. Vidal, R. C. Maury, and G. Guille, Basalts from Mururoa, Fangataufa and Gambier Islands (French Polynesia): Geochemical dependence on the age of the lithosphere, *Earth Planet Sci. Lett.*, *117*, 89–100, 1993.

Epp, D., and N. C. Smoot, Distribution of seamounts in the North Atlantic, *Nature*, *337*, 254–257, 1989.

Farley, K. A., and H. Craig, Mantle plumes and mantle sources: Technical comment, *Science*, *258*, 821, 1992.

Farley, K. A., J. H. Natland, and H. Craig, Binary mixing of enriched and undegassed (primitive?) mantle components (He, Sr, Nd, Pb) in Samoan lavas, *Earth Planet. Sci. Lett.*, *111*, 183–199, 1992.

Farnetani, C. G., and M. A. Richards, Thermal entrainment and melting in mantle plumes, *Earth Planet. Sci. Lett.*, *136*, 251–267, 1995.

Feighner, M. A., and K. S. Harpp, A fault model for the formation of the Wolf-Darwin Lineament, Galápagos, *Eos Trans. AGU*, *77*, 734, 1996.

Feighner, M. A., and M. A. Richards, The fluid dynamics of plume-ridge and plume-plate interactions: An experimental investigation, *Earth Planet. Sci. Lett.*, *129*, 171–182, 1995a.

Feighner, M. A., and M. A. Richards, Lithospheric structure and compensation mechanisms of the Galápagos Archipelago, *J. Geophys. Res.*, *99*, 6711–6729, 1995b.

Fornari, D. J., M. R. Perfit, J. F. Allan, R. Batiza, R. Haymon, A. Barone, W. B. F. Ryan, T. Smith, T. Simkin, and M. A. Luckman, Geochemical and structural studies of the Lamont seamounts: Seamounts as indicators of mantle processes, *Earth Planet. Sci. Lett.*, *89*, 63–83, 1988.

Gallahan, W. E., and R. L. Nielsen, The partitioning of Sc, Y, and the rare earth elements between high-Ca pyroxene and natural mafic to intermediate lavas at 1 atmosphere, *Geochim. Cosmochim. Acta*, *56*, 2387–2404, 1992.

Geist, D. J., An appraisal of melting processes and the Galápagos hotspot: Major and trace element evidence, *J. Volcanol. Geotherm. Res.*, *52*, 65–82, 1992.

Geist, D. J., W. M. White, and A. R. McBirney, Plume-asthenosphere mixing beneath the Galápagos archipelago, *Nature*, *333*, 657–660, 1988.

Geist, D. J., T. R. Naumann, and P. Larson, Evolution of Galápagos magmas: Mantle and crustal fractionation without assimilation, *J. Petrol.*, *39*, 953–971, 1998.

Graham, D. W., W. J. Jenkins, J.-G. Schilling, G. Thompson, M. D. Kurz, and S. E. Humphris, Helium isotope geochemistry of mid-ocean ridge basalts from the South Atlantic, *Earth Planet. Sci. Lett.*, *110*, 133–147, 1992.

Graham, D. W., D. M. Christie, K. S. Harpp, and J. E. Lupton, Mantle plume helium in submarine basalts from the Galápagos platform, *Science*, *262*, 2023–2026, 1993.

Griffiths, R. W., The differing effects of compositional and thermal buoyancies on the evolution of mantle diapirs, *Phys. Earth Planet. Inter.*, *43*, 261–273, 1986.

Griffiths, R. W., and M. A. Richards, The adjustment of mantle plumes to changes in plate motion, *Geophys. Res. Lett.*, *16*, 437–440, 1989.

Gripp, A. E., and R. G. Gordon, Current plate velocities relative to hotspots incorporating the NUVEL-1 global plate model, *Geophys. Res. Lett.*, *17*, 1109–1112, 1990.

Hanan, B. B., and D. W. Graham, Lead and helium isotope evidence from oceanic basalts for a common deep source of mantle plumes, *Science*, *272*, 991–995, 1996.

Harpp, K. S., Magmatic evolution of mid-ocean ridges and hotspots: Isotopic and trace element studies of the East Pacific Rise, Mid-Atlantic Ridge, and Galápagos Islands, Ph.D. thesis, Cornell Univ., Ithaca, N.Y., 1995.

Harpp, K. S., K. R. Wirth, J. S. Pistiner, D. J. Korich, and L. Mayhew, Plume-ridge interaction in the Galápagos: An example of hotspot-induced near-ridge volcanism at Genovesa Island (abstract), paper presented at the National Meeting, Geol. Soc. of Am., Reno, Nev., 2000.

Hart, S. R., The DUPAL anomaly: A large scale isotopic mantle anomaly in the Southern Hemisphere, *Nature*, *309*, 753–757, 1984.

Hart, S. R., Heterogeneous mantle domains: Signatures, genesis and mixing chronologies, *Earth Planet. Sci. Lett.*, *90*, 273–296, 1988.

Hart, S. R., and T. Dunn, Experimental cpx-melt partitioning of 24 trace elements, *Contrib. Mineral. Petrol.*, *113*, 1–8, 1992.

Hart, S. R., E. H. Hauri, L. A. Oschmann, and J. A. Whitehead, Mantle plumes and entrainment: Isotopic evidence, *Science*, *256*, 517–520, 1992a.

Hart, S. R., E. H. Hauri, L. A. Oschmann, and J. A. Whitehead, Mantle plumes and mantle sources: Technical comments, *Science*, *258*, 821–822, 1992b.

Hauri, E. H., J. A. Whitehead, and S. R. Hart, Fluid dynamic and geochemical aspects of entrainment in mantle plumes, *J. Geophys. Res.*, *99*, 24,275–24,300, 1994.

Hawkesworth, C. J., N. W. Rogers, P. W. C. van Calsteren, and M. A. Menzies, Mantle enrichment processes, *Nature*, *311*, 331–335, 1984.

Hawkesworth, C. J., P. Van Calsteren, N. W. Rogers, and M. A. Menzies, Isotope variations in recent volcanics: A trace-element perspective, in *Mantle Metasomatism*, 472 pp., Academic, San Diego, Calif., 1987.

Hey, R., Tectonic evolution of the Cocos-Nazca spreading center, *Geol. Soc. Am. Bull.*, *88*, 1404–1420, 1977.

Hilton, D. R., M. F. Thirwall, R. N. Taylor, B. J. Murton, and A. Nichols, Controls on magmatic degassing along the Reykjanes Ridge with implications for the helium paradox, *Earth Planet. Sci. Lett.*, *183*, 43–50, 2000.

Hirschmann, M. M., and E. M. Stolper, A possible role for garnet pyroxenite in the origin of the "garnet signature" in MORB, *Contrib. Mineral. Petrol.*, *124*, 185–208, 1996.

Hoernle, K. A., R. Werner, J. Phipps Morgan, J. Bryce, and J. Mrazek, Existence of complex spatial zonation in

the Galápagos plume for at least 14.5 Ma, *Geology*, *28*, 435–438, 2000.

Klein, E. M., and C. H. Langmuir, Ocean ridge basalt chemistry, axial depth, crustal thickness and temperature variations in the mantle, *J. Geophys. Res.*, *92*, 8089–8115, 1987.

Kurz, M. D., and D. J. Geist, Dynamics of the Galápagos hotspot from helium isotope geochemistry, *Geochim. Cosmochim. Acta*, *63*, 4139–4156, 1999.

Kurz, M. D., W. J. Jenkins, and S. R. Hart, Helium isotopic systematics of oceanic islands: Implications for mantle heterogeneity, *Nature*, *297*, 43–47, 1982a.

Kurz, M. D., W. J. Jenkins, J. G. Schilling, and S. R. Hart, Helium isotopic variations in the mantle beneath the central North Atlantic Ocean, *Earth Planet. Sci. Lett.*, *58*, 1–14, 1982b.

Kurz, M. D., W. J. Jenkins, S. Hart, and D. Clague, Helium isotopic variations in Loihi Seamount and the island of Hawaii, *Earth Planet. Sci. Lett.*, *66*, 388–406, 1983.

Kurz, M. D., T. Kenna, D. Kammer, J. M. Rhodes, and M. O. Garcia, Isotopic evolution of Mauna Loa volcano: A view from the submarine southwest rift, in *Mauna Loa Revealed: Structure, Composition, History, and Hazards, Geophys. Monogr. Ser.*, vol. 92, edited by J. P. Lockwood and J. M. Rhodes, pp. 289–306, AGU, Washington, D. C., 1995.

Langmuir, C. H., R. D. Voche Jr, G. N. Hanson, and S. R. Hart, A general mixing equation with applications to Icelandic basalts, *Earth Planet. Sci. Lett.*, *37*, 380–392, 1978.

Langmuir, C. H., E. M. Klein, and T. Plank, Petrological systematics of mid-ocean ridge basalts: Constraints on melt generation beneath ocean ridges, in *Mantle Flow and Melt Generation at Mid-Ocean Ridges, Geophys. Monogr. Ser.*, vol. 71, edited by J. P. Morgan, D. K. Blackman, J. M. Sinton, pp. 183–280, AGU, Washington, D. C., 1992.

Lassiter, J. C., E. H. Hauri, P. W. Reiners, and M. O. Garcia, Generation of Hawaiian post-erosional lavas by melting of a mixed lherzolite/pyroxenite source, *Earth Planet. Sci. Lett.*, *178*, 269–284, 2000.

LeMaitre, R. W., *Numerical Petrology: Statistical Interpretation of Geochemical Data, Develop. Petrol.*, vol. 8, 281 pp., Elsevier Sci., New York, 1982.

Mahoney, J. J., J. M. Sinton, M. D. Kurz, J. D. Macdougall, K. J. Spencer, and G. W. Lugmair, Isotope and trace element characteristics of a super-fast spreading ridge: East Pacific Rise, 13–23°S, *Earth Planet. Sci. Lett.*, *121*, 173–193, 1994.

Marriott, F. H. C., *The Interpretation of Multiple Observations*, 117 pp., Academic, San Diego, Calif., 1974.

McBirney, A. R., Differentiated rocks of the Galápagos hotspot, *J. Geol. Soc. London*, *76*, 61–69, 1993.

McKenzie, D. P., The extraction of magma from the crust and mantle, *Earth. Planet. Sci. Lett.*, *74*, 81–91, 1985.

McKenzie, D., Some remarks on the movement of small melt fractions in the mantle, *Earth Planet. Sci. Lett.*, *95*, 53–72, 1989.

McKenzie, D., and R. K. O'Nions, Partial melt distributions from inversion of rare earth element concentrations, *J. Petrol.*, *32*, 1021–1091, 1991.

Menzies, M. A., and V. R. Murthy, Mantle metasomatism as a precursor to the genesis of alkaline magmas: Isotopic evidence, *Am. J. Sci.*, *280A*, 622–638, 1980a.

Menzies, M. A., and V. R. Murthy, Nd and Sr isotope geochemistry of hydrous mantle nodules and their host alkali basalts: Implications for local heterogeneities in metasomatically veined mantle, *Earth Planet. Sci. Lett.*, *46*, 323–334, 1980b.

Morgan, W. J., Rodriguez, Darwin, Amsterdam. . ., A second type of hotspot island, *J. Geophys. Res.*, *83*, 5355–5360, 1978.

Nakamura, N., K. Yamamoto, S. Noda, Y. Nishikawa, H. Komi, H. Nagamoto, T. Nakayama, and K. Misawa, Determination of picogram quantities of rare-earth elements in meteoritic materials by direct-loading thermal ionization mass spectrometry, *Anal. Chem.*, *61*, 755–762, 1989.

Nielsen, R. L., A model for the simulation of combined major and trace element liquid lines of decent, *Geochim. Cosmochim. Acta*, *52*, 27–38, 1988.

Nielsen, R. L., and W. E. Gallahan, The partitioning of Sc, Y, and the rare earth elements between high-Ca pyroxene and natural mafic to intermediate lavas at 1 atmosphere, *Geochim. Cosmochim. Acta.*, *56*, 2387–2404, 1992.

O'Hara, M. J., Importance of the "shape" of the melting regime during partial melting of the mantle, *Nature*, *314*, 58–62, 1985.

Phipps Morgan, J., The generation of a compositional lithosphere by mid-ocean ridge melting and its effect on subsequent off-axis hotspot upwelling and melting, *Earth Planet. Sci. Lett.*, *146*, 213–232, 1997.

Plank, T., and C. H. Langmuir, Effects of the melting regime on the composition of the oceanic crust, *J. Geophys. Res.*, *97*, 19,719–19,770, 1992.

Prinzhofer, A., E. Lewin, and C. J. Allegre, Stochastic melting of the marble cake mantle: Evidence from local study of the East Pacific Rise at 12°50′N, *Earth Planet. Sci. Lett.*, *92*, 189–206, 1989.

Ribe, N. M., and U. R. Christensen, Three-dimensional modeling of plume-lithosphere interaction, *J. Geophys. Res.*, *99*, 669–682, 1994.

Richards, M. A., and R. W. Griffiths, Thermal entrainment by deflected mantle plumes, *Nature*, *342*, 900–902, 1989.

Roden, M. K., S. R. Hart, F. A. Frey, and W. G. Melson, Sr, Nd and Pb isotopic and REE geochemistry of St. Paul's rocks: The metamorphic and metasomatic development of an alkali basalt magma source, *Contrib. Mineral. Petrol.*, *85*, 376–390, 1984.

Schilling, J.-G., Upper mantle heterogeneities and dynamics, *Nature*, *314*, 62–67, 1985.

Schilling, J.-G., Fluxes and excess temperatures of mantle plumes inferred from their interaction with migrating mid-ocean ridges, *Nature*, *352*, 397–403, 1991.

Schilling, J.-G., R. H. Kingsley, and J. D. Devine, Galápagos hot spot-spreading center system, 1, Spatial petrological and geochemical variations (83°W–101°W), *J. Geophys. Res.*, *87*, 5593–5610, 1982.

Sen, G., F. A. Frey, N. Shimizu, and W. P. Leeman, Evolution of the lithosphere beneath Oahu, Hawaii: Rare earth element abundances in mantle xenoliths, *Earth Planet. Sci. Lett.*, *119*, 53–69, 1993.

Shen, Y., D. W. Forsyth, D. S. Scheirer, and K. C. Macdonald, Two forms of volcanism: Implications for mantle flow and off-axis crustal production on the west flank of the Southern East Pacific Rise, *J. Geophys. Res.*, *98*, 17,875–17,889, 1993.

Sinton, C. W., D. M. Christie, V. L. Coombs, R. L. Nielsen, and M. R. Fisk, Near-primary melt inclusions in anorthite phenocrysts from the Galápagos platform, *Earth Planet. Sci. Lett.*, *119*, 527–537, 1993.

Sinton, C., D. M. Christie, and R. A. Duncan, Geochronology of Galápagos seamounts, *J. Geophys. Res.*, *101*, 13,689–13,700, 1996.

Small, C., Observations of ridge-hotspot interactions in the Southern Ocean, *J. Geophys. Res.*, *100*, 17,931–17,946, 1995.

Staudacher, T., and C. J. Allègre, Recycling of oceanic crust and sediments: the noble gas subduction barrier, *Earth Planet. Sci. Lett.*, *89*, 173–183, 1988.

Staudigel, H., A. Zindler, S. R. Hart, T. Leslie, C. Y. Chen, and D. A. Clague, The isotope systematics of a juvenile inplate volcano: Pb, Nd and Sr isotope ratios of basalts from Loihi seamount, Hawaii, *Earth Planet. Sci. Lett.*, *69*, 13–29, 1984.

Stille, P., D. M. Unruh, and M. Tatsumoto, Pb, Sr, Nd, and Hf isotopic constraints on the origin of Hawaiian basalts and evidence for a unique mantle source, *Geochim. Cosmochim. Acta*, *50*, 2303–2320, 1986.

Sun, S. S., and W. F. McDonough, Chemical and isotopic systematics of oceanic basalts: Implications for mantle composition and processes, in *Magmatism in the Ocean Basins*, edited by A. D. Saunders, and M. J. Norry, Spec. Publ. 42, pp. 313–345, Geol. Soc. of Am., Boulder, Colo., 1989.

Verma, S. P., and J.-G. Schilling, Galápagos hot spot-spreading center system, 2, $^{87}Sr/^{86}Sr$ and large ion lithophile element variations (85°W–101°W), *J. Geophys. Res.*, *87*, 10,838–10,856, 1982.

Verma, S. P., J. G. Schilling, and D. G. Waggoner, Neodymium isotopic evidence for Galápagos hotspot-spreading centre system evolution, *Nature*, *306*, 654–657, 1983.

Wass, S. Y., and N. W. Rogers, Mantle metasomatism: Precursor to continental alkaline volcanism, *Geochim. Cosmochim. Acta*, *44*, 1811–1824, 1980.

White, W. M., The sources of ocean basalts: Radiogenic isotopic evidence, *Geology*, *13*, 115–118, 1985.

White, W. M., and A. W. Hofmann, Geochemistry of the Galápagos Islands: Implications for mantle dynamics and evolution, *Year Book Carnegie Inst. Washington*, *77*, 596–606, 1978.

White, W. M., A. R. McBirney, and R. A. Duncan, Petrology and geochemistry of the Galápagos Islands: Portrait of a pathological mantle plume, *J. Geophys. Res.*, *98*, 19,533–19,563, 1993.

Williams, D. L., R. P. Von Herzen, J. G. Sclater, and R. N. Anderson, The Galápagos Spreading Center: Lithospheric cooling and hydrothermal circulation, *R. Astron. Soc. Geophys. J.*, *38*, 587–608, 1974.

Wilson, D. S., and R. N. Hey, History of rift propagation and magnetization intensity for the Cocos-Nazca spreading center, *J. Geophys. Res.*, *100*, 10,041–10,056, 1995.

Wilson, J. T., A possible origin of the Hawaiian Islands, *Can. J. Phys.*, *41*, 863–870, 1963.

Zhang, Y.-S., and T. Tanimoto, Ridges, hotspots and their interaction as observed in seismic velocity maps, *Nature*, *355*, 45–49, 1992.

Zindler, A., and S. R. Hart, Chemical Geodynamics, *Ann. Rev. Earth Planet. Sci.*, *14*, 493–571, 1986.

Zindler, A., E. Jagoutz, and S. Goldstein, Nd, Sr and Pb-isotopic systematics in a three component mantle: A new perspective, *Nature*, *298*, 519–523, 1982.